An extension of the chemostat model with linear coupling between species *

Tewfik Sari, Radhouane Fekih-Salem

An extension of the chemostat model with linear coupling between species

Tewfik Sari* and Radhouane Fekih-Salem†

Abstract. We investigate the classical model of competition of two populations in the chemostat when a linear coupling between the populations is taken into account and the removal rates of the populations are distinct from the dilution rate and their yield coefficients are also distinct. This model extends a model of wall growth and a model of lateral gene transfer, previously studied in the literature. We show the existence and uniqueness of the coexistence equilibrium at which the populations coexist, provided that the input concentration of the chemostat exceeds a critical value, or, equivalently the dilution rate does not exceed a critical value that can be computed explicitly. In contrast with the particular cases of this model, previously studied in the literature, the positive equilibrium can be unstable with the appearance of Hopf bifurcations and sustainable oscillations. We construct the operating diagram of the system, which is the two-parameter bifurcation diagram with respect to the operating parameters, that are the dilution rate of the chemostat and its input nutrient concentration. This study reveals a rich variety of dynamical behaviours, including the emergence and disappearance of stable and unstable limit cycles through Hopf bifurcations and limit point of cycles bifurcations. Furthermore, codimension-two bifurcations such as cusp and generalized Hopf points are identified, highlighting complex transitions in the system's dynamics.

Key words. Chemostat, Competition, Mutation, Operating diagram, Wall growth.

MSC codes. 34A34 , 34D20 , 92B05 , 92D25

1. Introduction. The simultaneous development of the chemostat in 1950 by Monod [19] and Novick and Szilard [22] led to major advances in microbiology and population biology, using the technique of continuous culture of microorganisms, see the surveys of Fredrickson and Stephanopoulos [11] or Hoskisson and Hobbs [14]. Today, the chemostat plays an important role as a model in mathematical biology and the mathematical analysis of the model can be found in the monographs of Smith and Waltman [29] or Harmand et al. [13]. It is well known that two microbial populations competing for a single nutrient in a chemostat with time-invariant inputs cannot coexist in an equilibrium [11]. The corresponding chemostat type model takes the form

$$\begin{array}{rcl} x_1' &=& [f_1(S) - D_1]x_1, \\ x_2' &=& [f_2(S) - D_2]x_2, \\ S' &=& (S^0 - S)D - \frac{1}{Y_1} f_1(S)x_1 - \frac{1}{Y_2} f_2(S)x_2, \end{array} \tag{1.1}$$

where $x_1(t)$ and $x_2(t)$ are the concentrations of the competing microorganisms and $S(t)$ is the concentration of the nutrient, at time t. Here, S^0 denotes the concentration of the input nutrient and D denotes the dilution rate (flow rate/volume). The growth functions $f_i(S)$ are assumed to be increasing and satisfying $f_i(0) = 0$. Growth $f_i(S)$ is proportional to

*GreenOwl project team, Université Côte d'Azur, Inria, INRAE, CNRS-Sorbonne Université (LOV), Valbonne, France, (tewfik.sari@proton.me)

†LAMSIN, National Engineering School of Tunis, University of Tunis El Manar, Tunis, Tunisia. (radhouane.fekih-salem@enit.utm.tn)

consumption $f_i(S)/Y_i$ where the parameters Y_i, $i = 1, 2$, are yield constants. The removal rates D_i, $i = 1, 2$, of the microorganisms depend on the dilution rate D and take the form

$$D_i = \alpha_i D + \varepsilon_i, \qquad i = 1, 2, \tag{1.2}$$

where ε_i is the specific death rate of x_i and $\alpha_i \in [0, 1]$ is a parameter allowing us to decouple the Hydraulic Retention Time, HRT $= 1/D$ and the Solid Retention Time SRT $= 1/(\alpha_i D)$, see [5, 26]. Hence, values of the removal rates D_1 and D_2 that are greater than the dilution rate D of the chemostat or less than D are both of biological interest.

In addition to the washout equilibrium $E_0 = (0, 0, S^0)$, where both species are extinct, system (1.1) can only have the equilibria $E_1 = (x_1, 0, \lambda_1)$ and $E_2 = (0, x_2, \lambda_2)$, where $f_i(\lambda_i) = D_i$ and $x_i = \frac{Y_i D}{D_i}(S^0 - \lambda_i)$. In these equilibria, one of the species is extinct. Therefore, coexistence is not possible in an equilibrium. Note that in the non-generic case where there exists S^*, such that $f_1(S^*) = D_1$ and $f_2(S^*) = D_2$, there is a continuous line of coexistence equilibria, but this case cannot be expected to be found in nature. For details and complements, see [2, 13, 15, 16, 25, 29].

We modify the classical competition model (1.1) and include a linear coupling between species, by introducing parameters $r_1 > 0$ and $r_2 > 0$ for the rates of transfer from species x_1 to x_2, and x_2 to x_1, respectively. The equations of interest then are

$$\begin{aligned} x_1' &= [f_1(S) - D_1]x_1 - r_1 x_1 + r_2 x_2, \\ x_2' &= [f_2(S) - D_2]x_2 + r_1 x_1 - r_2 x_2, \\ S' &= (S^0 - S)D - \tfrac{1}{Y_1} f_1(S)x_1 - \tfrac{1}{Y_2} f_2(S)x_2. \end{aligned} \tag{1.3}$$

This extension of the classic model of competition in the chemostat encompasses several special cases that have been considered in the literature. The case $D_1 = D$, $D_2 = 0$ and $Y_1 = Y_2 = 1$ of (1.3) is the model of bacterial growth on the wall in a chemostat studied by Pilyugin and Waltman [23], where $x_1(t)$ and $x_2(t)$ are the concentrations of microorganisms at time t in the flow media and on the wall, respectively. The coefficients r_1 and r_2 are the rates of adhesion to and shearing from the wall. It is proved in [23] that, in this case the model has a coexistence equilibrium which is stable, if it exists. Another model where two microbial populations compete for a single resource in a chemostat but one of them exhibits attachment to the chemostat wall was studied by Baltzis and Fredrickson [3]. However, their model is not of the form (1.3) considered here.

Another interesting particular case of (1.3), obtained when $D_1 = D_2 = D$ and $Y_1 = Y_2$, is the case with two strains of the model of lateral gene transfer studied by De Leenheer et al. [17] and Bayen et al. [4], where $x_1(t)$ and $x_2(t)$ are the concentrations of the two competing strains of the microorganisms at time t, and r_1 and r_2 are interpreted now as the rates at which the strains convert from one type to another. It is proved in [4, 17] that the positive equilibrium is stable if it exists. Consequently, our results can also be seen as extensions of the results of [4, 17], in the case where there are only two strains.

In section 2.4, we will give more details on the comparisons between our results obtained for system (1.3) and those of [23] and [4, 17] obtained for the particular cases they considered. We obtain interesting and new phenomena that do not appear in the models considered in [4, 17, 23]. In particular, we show that for the more general model (1.3) the positive equilibrium

can be destabilized. Hence, in this work, we revisit the chemostat models in [4, 17, 23] by extending the assumptions they made. This extension, which consists of considering different yields Y_i or different removal rates D_i, will encompass situations of biological interest that are more extensive than the more restrictive conditions $Y_1 = Y_2$ and $D_1 = D, D_2 = 0$ considered in [23] or $Y_1 = Y_2$ and $D_1 = D_2 = D$ considered in [4, 17].

The parameters r_i, Y_i, α_i and ε_i, as well as the parameters in the growth functions $f_i(S)$, in system (1.3) where the D_i are given by (1.2) are called the *biological parameters* of the system, since they depend on the organisms and substrate considered. In contrast, the *operating parameters* of the system are the input concentration of the nutrient S^0 and the dilution rate D of the chemostat. These parameters are called operating parameters since they are under the control of the experimenter. Our aim is also to construct the operating diagram of the system, i.e., its two-parameter bifurcation diagram in the (S^0, D) parameter plane.

The paper is organized as follows. The main results are presented in section 2, while illustrative examples are discussed in section 3. The theoretical construction of the operating diagram is detailed in section 4, based on the existence and stability conditions of system (1.3). One- and two-parameter bifurcation diagrams, computed using MATCONT, are analyzed in section 5, revealing the emergence and disappearance of stable and unstable limit cycles via Hopf bifurcations and limit point of cycles (LPC) bifurcations. Section 6 concludes with a discussion of the main findings and their biological relevance. Additional numerical experiments and bifurcation diagrams illustrating various dynamical scenarios are provided in the Appendix.

2. Results.

The aim of this paper is to study system (1.3) where the removal rates D_1 and D_2 are given by (1.2). Recall that the yield coefficients Y_i in the classical competition chemostat model (1.1) can be normalized to 1, simply by replacing x_i by x_i/Y_i. If this change of variables is made on (1.3), we obtain a system where Y_1 and Y_2 are replaced by 1 in the equation of S, r_1 is maintained and r_2 is changed to r_2Y_2/Y_1, in the equation of x_1, while r_2 is maintained and r_1 is changed to r_1Y_1/Y_2, in the equation of x_2. Consequently, when equal, the yield coefficients Y_i in (1.3) can be normalized to 1. However, this normalization cannot be made when they are not equal.

2.1. Hypotheses and preliminary results.

We consider the following hypotheses.

Hypothesis 2.1. Growth functions $f_i(S)$ are assumed to be the following:
(i) $\mathcal{C}^1$-smooth with $f_i(0) = 0$,
(ii) a monotone function of S: $f_i'(S) \geq 0$ for $S > 0$. Moreover, for every $S > 0$, we have $f_1'(S) > 0$ or $f_2'(S) > 0$.

Hypothesis 2.2. At least one of the removal rates D_i is positive.

Using classical arguments in the mathematical theory of the chemostat, we can prove that the positive cone is positively invariant for (1.3) and that the solutions are uniformly bounded in forward time, see for example the proofs of [23, Lemmas 2.1 and 2.2] and [17, Lemma 1].

The operating parameters S^0 and D can be normalized to 1 as in [17, 23]. The usual scaling is to measure concentrations of S in units of S^0 and time in units of $1/D$. This yields the new system where the new $f_i(S)$ replaces $\frac{1}{D} f_i(S^0 S)$, the new Y_i, D_i and r_i are $S^0 Y_i$, D_i/D

and r_i/D, respectively. We will not make this reduction, as our objective is also to construct the operating diagram of the system, i.e. to describe the behaviour of the system as a function of the operating parameters S^0 and D.

Lemma 2.3. *In addition to the washout equilibrium $E_0 = (0, 0, S^0)$, system (1.3) can only have an equilibrium $E_1 = (x_1^*, x_2^*, S^*)$, with $x_1^* > 0$ and $x_2^* > 0$. If E_1 is such an equilibrium, then $\det(B(S^*)) = 0$, where $B(S)$ is given by*

$$B(S) = \begin{pmatrix} f_1(S) - D_1 - r_1 & r_2 \\ r_1 & f_2(S) - D_2 - r_2 \end{pmatrix}. \tag{2.1}$$

Let ρ_i, $i = 1, 2$, be defined by

$$\rho_i = \sup\{S : f_i(S) < D_i + r_i\}. \tag{2.2}$$

There exists no positive equilibrium $E_1 = (x_1^*, x_2^*, S^*)$, with $S^* \geq \min(\rho_1, \rho_2)$.

Proof. If $E_1 = (x_1^*, x_2^*, S^*)$ is an equilibrium of (1.3), then

$$-m_{11}x_1^* + r_2x_2^* = 0, \tag{2.3}$$

$$r_1x_1^* - m_{22}x_2^* = 0, \tag{2.4}$$

$$m_{31}x_1^* + m_{32}x_2^* = (S^0 - S^*)D, \tag{2.5}$$

where m_{31}, m_{32}, m_{11} and m_{22} are defined by

$$m_{11} = D_1 + r_1 - f_1(S^*),\ m_{22} = D_2 + r_2 - f_2(S^*),\ m_{31} = \tfrac{f_1(S^*)}{Y_1},\ m_{32} = \tfrac{f_2(S^*)}{Y_2}. \tag{2.6}$$

If $x_1^* = 0$, then equation (2.3) shows that $x_2^* = 0$. If $x_2^* = 0$, then equation (2.4) shows that $x_1^* = 0$. Therefore, besides $E_0 = (0, 0, S^0)$, system (1.3) can only have an equilibrium $E_1 = (x_1^*, x_2^*, S^*)$, with $x_1^* > 0$ and $x_2^* > 0$. If such an equilibrium exists, then system (2.3,2.4), which is a homogeneous linear system, has a non-trivial solution, if and only if the determinant of the system is zero, i.e. $\det(B(S^*)) = 0$, where $B(S)$ is given by (2.1).

If $\min(\rho_1, \rho_2) \leq S^* \leq \max(\rho_1, \rho_2)$, then $m_{11}m_{22} \leq 0$ and hence, $\det(B(S^*)) = m_{11}m_{22} - r_1r_2 < 0$. If $S^* \geq \max(\rho_1, \rho_2)$, then $m_{11} \leq 0$ and $m_{22} \leq 0$, so that the linear system (2.3,2.4) has nonnegative coefficients and hence, cannot have a positive solution. ∎

2.2. Existence of the positive equilibrium. The equation

$$\det(B(S)) = 0, \quad \text{for} \quad S \in I := [0, \min(\rho_1, \rho_2)), \tag{2.7}$$

plays an essential role in the discussion. This equation must be considered over the interval I since, according to Lemma 2.3, S^* must satisfy the condition $0 \leq S^* < \min(\rho_1, \rho_2)$.

Lemma 2.4. *Assume that Hypothesis 2.1 is satisfied. There exists a unique solution $S^* \in I$ of equation (2.7). If $D_1 = D_2 = 0$, then $S^* = 0$. If Hypothesis 2.2 is satisfied, then $S^* > 0$.*

Proof. Let $b(S) = \det(B(S))$. We have

$$b' = f_1'(f_2 - D_2 - r_2) + f_2'(f_1 - D_1 - r_1).$$

Using (2.2), $f_1 - D_1 - r_1 < 0$ and $f_2 - D_2 - r_2 < 0$, on I. Using Hypothesis 2.1, for every $S > 0$ in I, $b'(S) < 0$. Hence, the equation (2.7) can have at most one solution $S^* \in I$. We have $b(\rho_1) = b(\rho_2) = -r_1 r_2 < 0$. In addition, we have $b(0) = D_1 D_2 + D_1 r_2 + D_2 r_1$. If $D_1 = D_2 = 0$, then $b(0) = 0$ and hence, the unique solution is $S^* = 0$. If $D_1 > 0$ or $D_2 > 0$, then $b(0) > 0$ and hence there exists a unique solution $S^* \in I$, which must satisfy $S^* > 0$. ∎

Proposition 2.5. *Assume that Hypothesis 2.1 is satisfied. If $D_1 = D_2 = 0$, then system (1.3) has no positive equilibrium. If Hypothesis 2.2 is satisfied then the system has a unique equilibrium $E_1 = (x_1^*, x_2^*, S^*)$, where, $S^* > 0$ is the unique solution of equation (2.7) (see Lemma 2.4), and x_1^*, x_2^* are given by*

$$x_1^* = \frac{D\left(S^0 - S^*\right)}{m_{31} + m_{32}\frac{m_{11}}{r_2}}, \quad x_2^* = \frac{D\left(S^0 - S^*\right)}{m_{32} + m_{31}\frac{m_{22}}{r_1}}, ten \tag{2.8}$$

where m_{11}, m_{22}, m_{31} and m_{32} are defined by (2.6). This equilibrium is positive, i.e. $S^* < S^0$, if and only if at least one of the following conditions is satisfied

$$f_1(S^0) - D_1 - r_1 > 0, \tag{2.9}$$

$$f_2(S^0) - D_2 - r_2 > 0, \tag{2.10}$$

$$\left(f_1\left(S^0\right) - D_1 - r_1\right)\left(f_2\left(S^0\right) - D_2 - r_2\right) < r_1 r_2. \tag{2.11}$$

Proof. If $D_1 = D_2 = 0$, then $S^* = 0$. Therefore, $m_{31} = m_{32} = 0$ and equation (2.5) cannot have a solution.

If $D_1 > 0$ or $D_2 > 0$, then $S^* > 0$ and hence, using Hypothesis 2.1, we have $m_{31} > 0$ or $m_{32} > 0$. Solving (2.3) in x_2^* we obtain:

$$x_2^* = \tfrac{m_{11}}{r_2} x_1^*. \tag{2.12}$$

Replacing x_2^* in (2.5) and solving in x_1^* yields the expression for x_1^* in (2.8). Similarly, solving (2.4) in x_1^*, and replacing x_1^* in (2.5), and solving in x_2^* yields the expression for x_2^* in (2.8). Since $S^* < \min(\rho_1, \rho_2)$, the terms m_{11} and m_{22} in the denominators of x_1^* and x_2^*, respectively, are positive. Hence, using $m_{31} \geq 0$ and $m_{32} \geq 0$ and at least one of them is positive, the denominators are positive. Therefore, $x_1^* > 0$ and $x_2^* > 0$ if and only if $S^* < S^0$.

Finally, if (2.9) is satisfied, then $S^0 > \rho_1$, so that $S^0 > S^*$. If (2.10) is satisfied, then $S^0 > \rho_2$, so that $S^0 > S^*$. If (2.11) is satisfied, then $b\left(S^0\right) < 0$, so that $S^0 > S^*$. Conversely, if $S^0 > S^*$, then $b(S^0) < 0$, which implies (2.11), or $S^0 > \min(\rho_1, \rho_2)$, which implies (2.9) or (2.10). ∎

Remark 2.6. Let $\lambda = \min(\lambda_1, \lambda_2)$, where λ_i, $i = 1, 2$, are defined by

$$\lambda_i = \begin{cases} 0 & \text{if} \quad D_i = 0, \\ \sup\{S \geq 0 : f_i(S) < D_i\} & \text{if} \quad D_i > 0. \end{cases} \tag{2.13}$$

The component S^* of the positive equilibrium satisfies the following properties: if $\lambda_1 = \lambda_2$, then $S^* = \lambda_1 = \lambda_2$, and if $\lambda_1 \neq \lambda_2$, then

$$\min(\lambda_1, \lambda_2) < S^* < \min\left(\max(\lambda_1, \lambda_2), \min(\rho_1, \rho_2)\right).$$

where ρ_i are defined by (2.2). Indeed, we have

$$\left.\begin{array}{ll} \text{if } \lambda_1 = \lambda_2, & b(\lambda_1) = b(\lambda_2) = 0 \\ \text{if } \lambda_1 < \lambda_2, & b(\lambda_1) > 0 > b(\lambda_2) \\ \text{if } \lambda_2 < \lambda_1, & b(\lambda_2) > 0 > b(\lambda_1) \end{array}\right\} \begin{array}{l} \Longrightarrow \\ \Longrightarrow \end{array} \begin{array}{l} S^* = \lambda_1 = \lambda_2, \\ \min(\lambda_1, \lambda_2) < S^* < \max(\lambda_1, \lambda_2). \end{array}$$

Remark 2.7. If the growth function f_i is strictly increasing, and if $D_i < m_i$ where

$$m_i = \sup\{f_i(S) : S \geq 0\},$$

the number λ_i, defined by (2.13), is finite and satisfies $\lambda_i = f_i^{-1}(D_i)$. Similarly, if $D_i + r_i < m_i$, then ρ_i, defined by (2.2), is finite and satisfies $\rho_i = f_i^{-1}(D_i + r_i)$.

2.3. Stability of the equilibria. We can now give our main result on the conditions of existence and stability of the equilibria of (1.3). Throughout the rest of the paper, stable equilibrium is taken to mean hyperbolic and locally asymptotically stable, i.e., the eigenvalues of the Jacobian matrix are of negative real parts, and unstable is taken to mean that at least one eigenvalue of the Jacobian matrix is of positive real part.

Theorem 2.8. *Assume that Hypotheses 2.1 and 2.2 are satisfied. System (1.3) can have up to two equilibria:*

- *The washout equilibrium $E_0 = (0, 0, S^0)$, that always exists. If the three conditions (2.9), (2.10) and (2.11) are reversed and strict, then E_0 is stable. If at least one of the conditions (2.9), (2.10) or (2.11) is satisfied then E_0 is unstable.*
- *The positive equilibrium $E_1 = (x_1^*, x_2^*, S^*)$, where S^* is the unique $S^* \in I$ such that $\det(B(S^*)) = 0$, and x_1^*, x_2^* are given by (2.8), that exists if and only if one of the conditions (2.9), (2.10) or (2.11) is satisfied. The positive equilibrium E_1 is stable if and only if $c_1 c_2 - c_3 > 0$, where*

$$\begin{aligned} c_1 &= m_{11} + m_{22} + m_{33}, \\ c_2 &= m_{33}(m_{11} + m_{22}) + m_{31} m_{13} + m_{32} m_{23}, \\ c_3 &= m_{13}(m_{32} r_1 + m_{31} m_{22}) + m_{23}(m_{31} r_2 + m_{32} m_{11}). \end{aligned} \tag{2.14}$$

Here, m_{11}, m_{22}, m_{31}, m_{32}, are given by (2.6) and m_{13}, m_{23}, m_{33} are given by

$$m_{13} = f_1'(S^*) x_1^*, \ m_{23} = f_2'(S^*) x_2^*, \ m_{33} = D + \tfrac{f_1'(S^*)}{Y_1} x_1^* + \tfrac{f_2'(S^*)}{Y_2} x_2^*. \tag{2.15}$$

Proof. The stability of E_0 is determined by the eigenvalues of the Jacobian matrix

$$J_0 = \begin{pmatrix} f_1(S^0) - D_1 - r_1 & r_2 & 0 \\ r_1 & f_2(S^0) - D_2 - r_2 & 0 \\ -\frac{1}{Y_1} f_1(S^0) & -\frac{1}{Y_2} f_2(S^0) & -D \end{pmatrix}.$$

The eigenvalues of J_0 are $-D$ and the eigenvalues of the 2×2 matrix at the upper left, which is the matrix $B(S^0)$, where $B(S)$ is defined by (2.1). The eigenvalues of $B(S^0)$ are of negative real part if and only if

$$\det(B(S^0)) = \left(f_1\left(S^0\right) - D_1 - r_1\right)\left(f_2\left(S^0\right) - D_2 - r_2\right) - r_1 r_2 > 0, \tag{2.16}$$

$$\text{and } \operatorname{Tr}(B(S^0)) = f_1(S^0) - D_1 - r_1 + f_2(S^0) - D_2 - r_2 < 0. \tag{2.17}$$

Condition (2.16) is the reversed and strict inequality (2.11). From (2.16), we deduce that $f_1\left(S^0\right) - D_1 - r_1$ and $f_2\left(S^0\right) - D_2 - r_2$ have the same sign. Therefore, from (2.17) we deduce that $f_1\left(S^0\right) - D_1 - r_1 < 0$ and $f_2\left(S^0\right) - D_2 - r_2 < 0$, which are the reversed and strict inequalities (2.9) and (2.10), respectively. Hence, we have proved that if the three conditions (2.9), (2.10) and (2.11) are reversed and strict, then E_0 is stable. Conversely, if (2.11) is satisfied, then $\det(B(S^0)) < 0$ and E_0 is unstable. If both (2.9) and (2.10) are satisfied, then $\mathrm{Tr}(B(S^0)) > 0$ and E_0 is unstable. If (2.9) is satisfied and (2.10) is reversed, then $\det(B(S^0)) < 0$ and E_0 is unstable. Similarly, if (2.10) is satisfied and (2.9) is reversed, then $\det(B(S^0)) < 0$ and E_0 is unstable. Hence, we have proved that if one of the conditions (2.9), (2.10) or (2.11) is satisfied, then E_0 is unstable.

The stability of $E_1 = (x_1^*, x_2^*, S^*)$ is determined by the eigenvalues of the Jacobian matrix

$$J_1 = \begin{pmatrix} -m_{11} & r_2 & m_{13} \\ r_1 & -m_{22} & m_{23} \\ -m_{31} & -m_{32} & -m_{33} \end{pmatrix}$$

where m_{ij} are defined by (2.6) and (2.15). Notice that we have used the opposite sign for some of the entries of J_1, so that all coefficients m_{ij} involved in the computations become positive, which will simplify the analysis of the characteristic polynomial of J_1. Also notice that $m_{11}m_{22} - r_1r_2 = \det(B(S^*)) = 0$.

The characteristic equation of J_1 is given by:

$$z^3 + c_1z^2 + c_2z + c_3 = 0, \tag{2.18}$$

where c_1, c_2 and c_3 are defined by (2.14). According to the Routh-Hurwitz criteria, E_1 is stable if and only if $c_1 > 0$, $c_3 > 0$ and $c_1c_2 - c_3 > 0$. Notice that $c_1 > 0$ and $c_3 > 0$. Therefore, E_1 is stable if and only if $c_1c_2 - c_3 > 0$. ∎

Remark 2.9. Using (2.14), the coefficients of the characteristic equation (2.18) are positive. Therefore, there is at least one negative real eigenvalue and no positive real eigenvalues, which implies that, in case of instability, the eigenvalues with positive real parts must be a complex conjugate pair.

2.4. Comparison with previous results. The results in Proposition 2.5 and Theorem 2.8 on the existence of E_1 and the stability of E_0 extend [23, Lemma 3.1 and Lemma 3.2] to the case where $D_1 \neq D$, $D_2 \neq 0$ and $Y_1 \neq Y_2$. They also extend the results of [4, 23] obtained when $D_1 = D_2 = D$. Let us give a quick overview of the method used in [23] for the study of the conditions of existence of E_1.

Proposition 2.10. *We assume that f_1 and f_2 are strictly increasing. A positive equilibrium exists if and only if the graphs of the functions*

$$F(S) = \frac{f_2(S) - D_2 - r_2}{f_2(S) - D_2} \quad \text{and} \quad G(S) = \frac{r_1}{f_1(S) - D_1}, \tag{2.19}$$

intersect at some point S^*, $0 < S^* < S^0$.

Proof. Adding the equations (2.3) and (2.4), we obtain $x_2^* = \frac{D_1 - f_1(S)}{f_2(S) - D_2} x_1^*$, which, when substituted in (2.4), yields

$$x_1^* \left((f_2(S) - D_2 - r_2) \frac{D_1 - f_1(S)}{f_2(S) - D_2} + r_1 \right) = 0.$$

After cancelling x_1^*, and dividing by $D_1 - f_1(S)$, we obtain the equation $F(S) = G(S)$, where $F(S)$ and $G(S)$ are defined by (2.19). $F(S)$ is a monotone increasing function of S and has an asymptote at $S = \lambda_2 := f_2^{-1}(D_2)$, while $G(S)$ is a monotone decreasing function of S and has an asymptote at $S = \lambda_1 := f_1^{-1}(D_1)$. A positive equilibrium corresponds to an intersection of the graphs of F and G at some point S^*, such that $0 < S^* < S^0$. We do not give more details on this approach. For more information, see [23, Fig. 3.1], obtained in the case $D_1 = D$ and $D_2 = 0$. ∎

When we apply this method to our more general case, where the functions f_i are not assumed to be strictly increasing, we need to take a few precautions in cases where the denominators of the functions F or G are not defined. Note that the equation $F(S) = G(S)$, where F and G are given by (2.19), is equivalent to the equation

$$(f_1(S) - D_1)(f_2(S) - D_2 - r_2) = (f_2(S) - D_2) r_1,$$

which is equivalent to the equation $(f_1(S) - D_1 - r_1)(f_2(S) - D_2 - r_2) = r_1 r_2$, that is, $\det(B(S)) = 0$.

Following [17], we can also obtain the result on the existence of E_1 by using Perron-Frobenius theory. Since the matrix $B(S)$, defined by (2.1), has off-diagonal positive entries, from the Perron-Frobenius theorem, we know that its spectral abscissa, i.e. the maximum of the real parts of its eigenvalues, is an eigenvalue of $B(S)$, denoted $\lambda_{max}(B(S))$, which is simple and has a corresponding positive eigenvector. Except for this positive eigenvector and its scalar multiples with a positive scalar, there are no other non-negative eigenvectors.

Proposition 2.11. *A positive equilibrium exists if and only if there exists $S^* \in (0, S^0)$ such that $\lambda_{max}(B(S^*)) = 0$. Such an S^* exists if and only if $\lambda_{max}(B(S^0)) > 0$.*

Proof. The linear system (2.3,2.4) can be written $B(S^*)x^* = 0$, where the matrix $B(S)$ is defined by (2.1) and $x^* = (x_1^*, x_2^*)^\top$. If $x^* \neq 0$, this means that 0 is an eigenvalue of $B(S^*)$ and x^* is a corresponding eigenvector. Since x^* is non-negative, it must be an eigenvector corresponding to $\lambda_{max}(B(S^*))$. Hence, if an equilibrium (S^*, x_1^*, x_2^*) exists with $x^* \neq 0$, then, necessarily equation $\lambda_{max}(B(S^*)) = 0$. is satisfied and, moreover, x^* must be a positive vector (rather than only non-negative). It is a well-known property that the spectral abscissa is increasing with the entries of a matrix which is positive off-diagonal. This property can also be obtained by straightforward computations from the following explicit expression of the spectral abscissa: $\lambda_{max}(B(S)) = \frac{\phi_1(S) + \phi_2(S) + \sqrt{\Delta(S)}}{2}$, where $\phi_i(S) = f_i(S) - D_i - r_i$ and $\Delta(S) = (\phi_1(S) - \phi_2(S))^2 + 4 r_1 r_2 > 0$. Therefore, $\frac{d}{dS}\lambda_{max}(B(S)) > 0$. Moreover, we have $\det(B(0)) > 0$ and $\mathrm{Tr}(B(0)) < 0$. Therefore, $\lambda_{max}(B(0)) < 0$. Equation (2.5) shows that S^* must satisfy the condition $S^* < S^0$. Hence, there exists a unique $S^* \in (0, S^0)$ such that $\lambda_{max}(B(S^*)) = 0$ if and only if equation $\lambda_{max}(B(S^0)) > 0$ is satisfied. ∎

This condition $\lambda_{max}(B(S^0)) > 0$ is equivalent to

$$\det(B(S^0)) < 0 \quad \text{or} \quad \det(B(S^0)) > 0 \text{ and } \operatorname{Tr}(B(S^0)) > 0. \tag{2.20}$$

We can easily see that the necessary and sufficient condition (2.20) of existence of the positive equilibrium is satisfied if and only if one of the conditions (2.9), (2.10) or (2.11) is satisfied. The result of Proposition 2.11 was obtained in [17] in the general case of n strains x_i, with $D_i = D$ for $i = 1, \dots, n$, under the assumption that the transfer matrix between strains is irreducible. We can see that the result remains true when the removal rates are not equal to the dilution rate [28].

In this section, we have seen that the results on the existence of a positive equilibrium extend those of [4, 17, 23]. These authors placed themselves in conditions where the positive equilibrium is stable as soon as it exists. Under the more general assumptions considered in this work, the stability of the positive equilibrium does not always occur.

2.5. Instability of the positive equilibrium. We now give a necessary and sufficient condition for the stability of E_1, which is easier to handle than the condition $c_1c_2 - c_3$ given in Theorem 2.8.

Remark 2.12. In this section, we denote by $S^* = S^*(D)$ the unique solution of equation $\det(B(S)) = 0$ to recall its dependence on the operating parameter D. In fact, $S^*(D)$ depends only on D and not on the operating parameter S^0, since the matrix $B(S)$ depends only on D and not on S^0. Therefore, the coefficients m_{11}, m_{22}, m_{31}, and m_{32}, defined by (2.6), depend only on D.

We consider the polynomial

$$P(X) = a(D)X^2 + b(D)X + c(D), \tag{2.21}$$

where

$$\begin{aligned}
a(D) &= a_{33}(a_{33}(m_{11} + m_{22}) + a_{13}m_{31} + a_{23}m_{32}),\\
b(D) &= a_{33}(m_{11} + m_{22})^2 + a_{13}m_{31}m_{11} + a_{23}m_{32}m_{22}\\
&\quad + D(a_{13}m_{31} + a_{23}m_{32} + 2a_{33}(m_{11} + m_{22})) - a_{13}r_1m_{32} - a_{23}r_2m_{31},\\
c(D) &= D(m_{11} + m_{22})(D + m_{11} + m_{22}),
\end{aligned}$$

where a_{13}, a_{23} and a_{33} are given by

$$a_{13} = f_1'(S^*), \quad a_{23} = f_2'(S^*)\tfrac{m_{11}}{r_2}, \quad a_{33} = \tfrac{f_1'(S^*)}{Y_1} + \tfrac{f_2'(S^*)}{Y_2}\tfrac{m_{11}}{r_2}, \tag{2.22}$$

and m_{ij} are defined by (2.6). Notice that $a(D) > 0$, $c(D) > 0$, and there are two negative terms in $b(D)$. Therefore, $b(D)$ can be negative. The polynomial $P(X)$ can be negative for positive values of X if and only if there exists D such that $b(D) < 0$ and $\Delta(D) := b^2(D) - 4a(D)c(D) > 0$. We define the set

$$I_1 := \{D > 0 : b(D) < 0 \text{ and } \Delta(D) > 0\}. \tag{2.23}$$

Note that I_1 is an open set. If $D \in I_1$ we denote by

$$X_1(D) = \tfrac{-b(D) - \sqrt{\Delta(D)}}{2a(D)} \text{ and } X_2(D) = \tfrac{-b(D) + \sqrt{\Delta(D)}}{2a(D)}$$

the roots of $P(X)$. They are real and positive. We have the following result:

Proposition 2.13. *The coexistence equilibrium E_1 can be unstable only if the set I_1 defined by (2.23) is not empty. If this condition holds then E_1 is unstable if and only if $D \in I_1$ and $F_1(D) < S^0 < F_2(D)$ where $F_1(D)$ and $F_2(D)$ are given by*

$$F_i(D) = S^*(D) + \frac{1}{D}\left(m_{31} + \frac{m_{32}m_{11}}{r_2}\right) X_i(D), \quad i = 1, 2. \tag{2.24}$$

Proof. The components x_1^* and x_2^*, given by (2.8) also depend on S^0. Notice that only the coefficients m_{13}, m_{23} and m_{33} in (2.15) are depending on x_1^* or x_2^*. If we replace x_2^* by its expression (2.12) in (2.15), we obtain

$$m_{13} = a_{13}x_1^*, \quad m_{23} = a_{23}x_1^*, \quad m_{33} = D + a_{33}x_1^*,$$

where a_{13}, a_{23} and a_{33} are given by (2.22). Straightforward computation show that $c_1c_2 - c_3 = P(x_1^*)$, where the polynomial $P(X)$ is defined by (2.21). E_1 is unstable if and only if $P(x_1^*) < 0$.

The product of the roots of $P(X)$, which is equal to $c(D)/a(D)$, is positive. Hence, the roots can be real and positive if and only if $b(D) < 0$ and $\Delta(D) > 0$, that is to say $D \in I_1$. If I_1 is not empty and $D \in I_1$ then $P(X)$ has two positive roots denoted $0 < X_1(D) < X_2(D)$. Note that $P(X) < 0$ if and only if $X_1(D) < X < X_2(D)$. Replacing X by x_1^* and using the formula (2.8) giving x_1^*, we see that the condition $X_1(D) < X < X_2(D)$ is equivalent to the condition $F_1(D) < S^0 < F_2(D)$ where $F_1(D)$ and $F_2(D)$ are given by (2.24). ∎

It is much easier to use the stability conditions in Proposition 2.13 than the $c_1c_2 - c_3 > 0$ condition in Theorem 2.8. In fact, the study of stability is reduced to the study of the signs of the functions $b(D)$ and $\Delta(D)$, of the single variable D. We will illustrate this in section 3.

2.6. Stability of the positive equilibrium.

Proposition 2.14. *The positive equilibrium of system (1.3), when it exists, is stable in the following three cases:*

1. *$D_1 = D$, $D_2 = 0$ and $Y_1 = Y_2 = 1$.*
2. *$f_2 = 0$ (or $f_1 = 0$).*
3. *$D_1 = D_2 = D$ and $Y_1 = Y_2 = 1$.*

Proof. The first case is the model considered in [23]. As shown in [23, pages 1559-1560], we have $c_1c_2 - c_3 > 0$. Hence, E_1 is stable if it exists [23, Lemma 3.3].

In the second case, if $f_2 = 0$, then the term $-a_{13}r_1m_{32} - a_{23}r_2m_{31}$ in $b(D)$ is equal to 0. Indeed, using (2.6) and (2.22), we have $m_{32} = 0$ and $a_{23} = 0$. Hence, $b(D) > 0$ for all D, so that, using Proposition 2.13, E_1 is always stable.

In the third case, using the variables (x_1, x_2, z), where $z = x_1 + x_2 + S$, the system becomes:

$$\begin{aligned} x_1' &= [f_1(z - x_1 - x_2) - D]x_1 - r_1x_1 + r_2x_2, \\ x_2' &= [f_2(z - x_1 - x_2) - D]x_2 + r_1x_1 - r_2x_2, \\ z' &= (S^0 - z)D. \end{aligned} \tag{2.25}$$

The positive equilibrium, becomes $E_1 = (x_1^*, x_2^*, S^0)$ and we have $S^0 = x_1^* + x_2^* + S^*$. The

Jacobian matrix at the positive equilibrium is written

$$J_1 = \begin{pmatrix} -m_{11} - m_{13} & r_2 - m_{13} & m_{13} \\ r_1 - m_{23} & -m_{22} - m_{23} & m_{23} \\ 0 & 0 & -D \end{pmatrix},$$

where m_{11} and m_{22}, given by (2.6), with $D_1 = D_2 = D$, and m_{13} and m_{23}, given by (2.15), are all positive. The eigenvalues of J_1 are $-D$, together with the eigenvalues of the matrix

$$C = \begin{pmatrix} -m_{11} - m_{13} & r_2 - m_{13} \\ r_1 - m_{23} & -m_{22} - m_{23} \end{pmatrix}.$$

We have $\mathrm{Tr}(C) = -m_{11} - m_{13} - m_{22} - m_{23} < 0$ and, since $m_{11}m_{22} - r_1 r_2 = 0$,

$$\det(C) = m_{13}m_{22} + m_{23}m_{11} + r_1 m_{13} + r_2 m_{23} > 0.$$

Therefore, the eigenvalues of C are of negative real parts. ∎

Remark 2.15. In the case where $f_2 = 0$, we know from Proposition 2.14 that E_1 is stable if it exists. Using a Lyapunov function, it is known that if $D_1 = D$, $D_2 = 0$, and $f_2 = 0$, then E_1 is a global attractor [23, Theorem 6.1]. This result remains true in the more general case where $f_2 = 0$ and D, D_1, D_2 are arbitrary, as shown in the following proposition.

Proposition 2.16 (Pilyugin[1]). *Consider the system* (1.3)*, with* $f_2 = 0$*, i.e.:*

$$\begin{aligned} x_1' &= [f_1(S) - D_1 - r_1]x_1 + r_2 x_2, \\ x_2' &= -(D_2 + r_2)x_2 + r_1 x_1, \\ S' &= (S^0 - S)D - \tfrac{1}{Y_1} f_1(S) x_1, \end{aligned} \tag{2.26}$$

and suppose that the positive equilibrium E_1 *exists. Then* E_1 *is GAS.*

Proof. The components of $E_1 = (x_1^*, x_2^*, S^*)$ satisfy the following two equations

$$f_1(S^*) - D_1 - r_1 = -r_2 x_2^*/x_1^*, \qquad D_2 + r_2 = r_1 x_1^*/x_2^*.$$

Therefore, we can rewrite the system (2.26), as

$$\begin{aligned} x_1' &= x_1(f_1(S) - f_1(S^*)) + \tfrac{r_2}{x_1^*}(-x_2^* x_1 + x_1^* x_2), \\ x_2' &= \tfrac{r_1}{x_2^*}(x_2^* x_1 - x_1^* x_2), \\ S' &= (S^0 - S)D - \tfrac{1}{Y_1} f_1(S) x_1. \end{aligned}$$

Let

$$W = Y_1 \frac{x_1^*}{r_2} \int_{S^*}^{S} \frac{f_1(z) - f_1(S^*)}{f_1(z)} dz + \frac{x_1^*}{r_2} \int_{x_1^*}^{x_1} \frac{z - x_1^*}{z} dz + + \frac{x_2^*}{r_1} \int_{x_2^*}^{x_2} \frac{z - x_2^*}{z} dz.$$

[1] S.S. Pilyugin (2025), A Lyapunov function for the case where $f_2 = 0$ and D, D_1, D_2 are arbitrary. Personal communication.

The derivative of W with respect to (2.26) is given by

$$\begin{aligned}\frac{dW}{dt} =& \frac{x_1^*}{r_2}\frac{f_1(S)-f_1(S^*)}{f_1(S)}(Y_1(S^0-S)D - f_1(S)x_1) + \frac{x_1^*}{r_2}(x_1-x_1^*)(f_1(S)-f_1(S^*))\\ &+ \frac{x_1-x_1^*}{x_1}(-x_2^*x_1+x_1^*x_2) + \frac{x_2-x_2^*}{x_2}(x_2^*x_1-x_1^*x_2)\\ =& \frac{x_1^*}{r_2}\frac{f_1(S)-f_1(S^*)}{f_1(S)}(Y_1(S^0-S)D - f_1(S)x_1^*) - \frac{(x_2^*x_1-x_1^*x_2)^2}{x_1x_2}.\end{aligned}$$

Using $f_2 = 0$, Hypothesis 2.1 implies that $f_1'(S) > 0$ for all $S > 0$. It follows that the first term is ≤ 0 with the inequality being strict unless $S = S^*$. Hence, W is a Lyapunov function and E_1 is GAS. ∎

3. Examples. We have seen in Proposition 2.14 cases where the positive equilibrium is stable if it exists. Let us give examples showing that this property is no longer true when the assumptions of this proposition are weakened. For this, we consider system (1.3) with linear growth functions $f_1(S) = a_1S$ and $f_2(S) = a_2S$, and the values of the biological parameters given in Table 1. In Appendix A.1 we perform numerical experiments to determine the signs of $b(D)$ and $\Delta(D)$ and then, the interval I_1 defined by (2.23). Since all the values of the biological parameters are fixed, these functions depend only on D and it is easy to find their zeros and study their signs.

Table 1

Values of biological parameters used in Examples 3.1, 3.2, 3.3, 3.4 and Fig. 1 for (1.3) with $f_i(S) = a_iS$ and $D_i = \alpha_iD + \varepsilon_i$, $i = 1, 2$, $\alpha_1 = 1$. The last column shows I_1 defined by (2.23).

Figure	a_1	a_2	Y_1	Y_2	r_1	r_2	ε_1	α_2	ε_2	I_1
1(a,b,c)	0.01	1	0.01	20	0.01	10	0	1	0	(0.271,1.844)
1(d)	0.6	0.4	1	1	6	0.01	5	1	8	(0,0.048)
1(e)	0.01	3	0.02	600	0.001	5	0	0	0	(0.039, 0.839)
1(f)	0.6	0.4	1	1	6	0.01	5	0	8	(0,0.049)

Example 3.1. Equal removal rates and different yields. Values of biological parameters are given in line 1 of Table 1. Since $I_1 \neq \emptyset$, the positive equilibrium can be unstable. Hence, the result of Proposition 2.14 that the positive equilibrium is stable if it exists obtained when $Y_1 = Y_2$ does not hold when the yields are distinct.

Example 3.2. Different removal rates and equal yields. Values of biological parameters are given in line 2 of Table 1. Since $I_1 \neq \emptyset$, the result of Proposition 2.14 that the positive equilibrium is stable if it exists obtained when $D_1 = D_2 = D$ does not hold when the removal rates are distinct.

Example 3.3. Different yields, $D_1 = D$ and $D_2 = 0$. Values of biological parameters are given in line 3 of Table 1. Since $I_1 \neq \emptyset$, the result of [23, Lemma 3.3] that the positive equilibrium is stable if it exists obtained when $Y_1 = Y_2 = 1$ does not hold when the yields are distinct.

Example 3.4. Equal yields, $D_1 \neq D$ and $D_2 \neq 0$. Values of biological parameters are given in line 4 of Table 1. Since $I_1 \neq \emptyset$, the result of [23, Lemma 3.3] that the positive equilibrium is stable if it exists obtained when $D_1 = D$ and $D_2 = 0$ does not hold when decay terms are added.

In the next section, we apply Proposition 2.13 and determine the set of operating parameters D and S^0 for which E_1 is unstable.

4. Operating diagrams.

The conditions of existence and stability of the equilibria of (1.3) given in Theorem 2.8 are summarized in Table 2. Therefore, the curves of the operating

Table 2

Existence and local stability of equilibria of (1.3)*, where* c_1*,* c_2 *and* c_3 *are defined by* (2.14) *and* $\phi_1 = f_1(S^0) - D_1 - r_1$*,* $\phi_2 = f_2(S^0) - D_2 - r_2$*,* $\phi_3 = \phi_1\phi_2 - r_1r_2$*.*

Equilibria	Existence	Local stability
E_0	Always	$\phi_1 < 0$ and $\phi_2 < 0$ and $\phi_3 > 0$
E_1	$\phi_1 > 0$ or $\phi_2 > 0$ or $\phi_3 < 0$	$c_1c_2 - c_3 > 0$

parameter plane defined by

$$\Phi_1 := \left\{\left(S^0, D\right) : \phi_1 = 0\right\}, \quad \Phi_2 := \left\{\left(S^0, D\right) : \phi_2 = 0\right\},$$
$$\Phi_3 := \left\{\left(S^0, D\right) : \phi_3 = 0\right\}, \quad \Phi_4 := \left\{\left(S^0, D\right) : c_1c_2 - c_3 = 0\right\},$$

play an essential role in the construction of the operating diagram. Curves Φ_1, Φ_2, and Φ_3 are easy to construct because their equations are simple. To construct the curve Φ_4 we will use Proposition 2.13. We first determine the open set I_1 defined by (2.23). To each connected component of I_1 corresponds a connected component of Φ_4. More precisely, we have the following result:

Proposition 4.1. *Let* (D^-, D^+) *be a connected component of* I_1*. If* $D^+ > D^- > 0$*, then* Φ_4 *has a compact component which is homeomorphic to the circle. If* $D^+ > D^- = 0$*, then* Φ_4 *has an unbounded component which goes to infinity as* $D \to 0$*.*

Proof. The boundary of I_1 is defined by $b(D) = 0$ or $\Delta(D) = 0$. If $b(D^+) = 0$, then, from the definition of $\Delta(D)$, $\Delta(D^+) < 0$. Thus $\Delta(D) < 0$ for $D < D^+$ close to D^+, so $D \notin I_1$. Hence, $b(D^+) \neq 0$ and we necessarily have $\Delta(D^+) = 0$. Similarly, if $D^- > 0$, we necessarily have $\Delta(D^-) = 0$. Hence, the roots $X_1(D)$ and $X_2(D)$ of $P(X)$ satisfy $X_1(D) = X_2(D)$ for $D = D^-$ and $D = D^+$. Thus, $F_1(D) = F_2(D)$ for $D = D^-$ and $D = D^+$. Since, in addition $F_1(D) < F_2(D)$ for $D^- < D < D^+$, we deduce that the corresponding component of Φ_4 defined by $S^0 = F_1(D)$ or $S^0 = F_2(D)$ is homeomorphic to the circle. If $D^- = 0$, then $c(D^-) = 0$. Therefore, $X_1(D^-) = 0$ and $X_2(D^-) = \frac{-b(D^-)}{a(D^-)} > 0$. Therefore, $F_2(D) \to +\infty$ as $D \to 0$. ∎

4.1. Linear growth.

For linear growth functions $f_i(S) = a_iS$, Φ_1 and Φ_2 curves are straight lines, while Φ_3 is a hyperbola admitting Φ_1 and Φ_2 as asymptotes. For the parameter values in Example 3.1, Figure 1(a) shows the signs of ϕ_1 and ϕ_2, while Figure 1(b) shows the signs of ϕ_3. We see that the condition ($\phi_1 < 0$ and $\phi_2 < 0$ and $\phi_3 > 0$) of stability of E_0

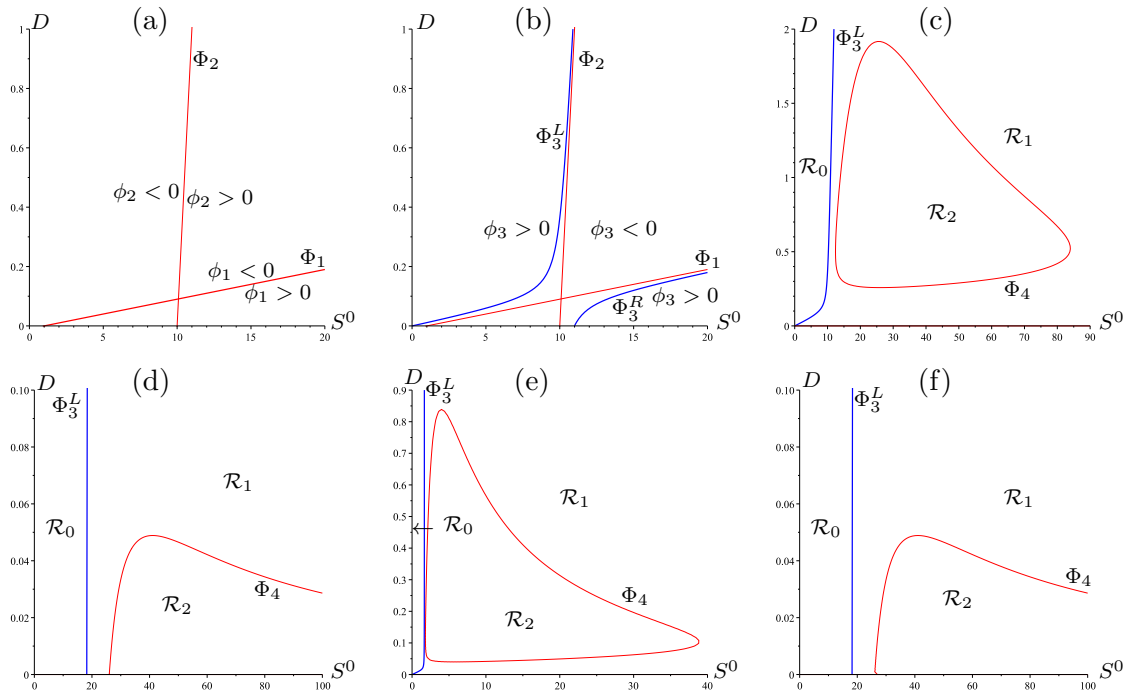

Figure 1. *(a,b) The curves Φ_i (in red), the curve $\Phi_3 = \Phi_3^L \cup \Phi_3^R$ (in blue) and the signs of ϕ_1, ϕ_2 and ϕ_3. (c,d,e,f) Operating diagram of (1.3). The asymptotic behaviour of (1.3) in the regions $\mathcal{R}_0$, $\mathcal{R}_1$ and $\mathcal{R}_2$ is given in Table 3. Biological parameter values are given in Table 1.*

Table 3

Existence and stability of equilibria of (1.3) in the regions $\mathcal{R}_0$, $\mathcal{R}_1$ and $\mathcal{R}_2$ of the operating diagrams shown in Figure 1(c,d,e,f) and Figure 2(c,d,e,f).

Region	E_0	E_1
$\mathcal{R}_0$	S	
$\mathcal{R}_1$	U	S
$\mathcal{R}_2$	U	U

is satisfied at the left of the component Φ_3^L of the hyperbola, while the condition ($\phi_1 > 0$ or $\phi_2 > 0$ or $\phi_3 < 0$) of existence of E_1 (and instability of E_0) is satisfied at right of Φ_3^L. Therefore, the curves Φ_3^L and Φ_4 separate the operating plane (S^0, D) in the three regions shown in Figure 1(c). Moreover, since $I_1 = (0.271, 1.844)$, Φ_4 is homeomorphic to the circle by Proposition 4.1, as it is seen on the figure. The asymptotic behaviour of (1.3) is described in Table 3.

Similarly, for the parameter values in Example 3.2, since $I_1 = (0, 0.048)$, Φ_4 is unbounded by Proposition 4.1. The curves Φ_3^L and Φ_4 separate the operating plane (S^0, D) in the three regions shown in Figure 1(d).

The operating diagrams for Examples 3.3 and 3.4 are presented in Figure 1(e) and (f), respectively. By Proposition 4.1 and the form of I_1, Φ_4 is homeomorphic to the circle in Example 3.3 and unbounded in Example 3.4.

Remark 4.2. A transcritical bifurcation occurs when the curve Φ_3^L is crossed by (S^0, D)

in which the stability of E_0 is transferred to E_1, which emerges stable into the interior of the positive cone. Moreover, a Hopf bifurcation is expected to occur when crossing the curve Φ_4. Indeed, by the Routh-Hurwitz criterion and since we showed that when E_1 exists, c_1 and c_3 are always positive, a Hopf bifurcation occurs when the expression $c_1c_2 - c_3$ changes sign as a parameter varies and if the so-called transversality conditions are satisfied: the real parts of a pair of complex eigenvalues with non zero imaginary part pass through 0 and change sign and the derivative of the real part of the eigenvalues with respect to the bifurcation parameter is non-zero when evaluated at the critical value when the real parts are zero. The nature of the bifurcation (subcritical or supercritical) is determined by evaluating the first Lyapunov coefficient. Since it is generally difficult to verify these conditions analytically, we will examine the occurrence of Hopf bifurcations only numerically for specific growth functions and when the biological parameters are fixed; see section 5.

Remark 4.3. Curve Φ_3^L has the equation $S^0 = S^*(D)$, where $S^*(D)$ is the smallest solution of the equation $\phi_3 = 0$. For linear growth functions, this equation is written $\alpha(S^0)^2 - \beta S^0 + \gamma = 0$, where $\alpha = a_1a_2$, $\beta = a_1(D_2 + r_2) + a_2(D_1 + r_1)$ and $\gamma = D_1D_2 + D_1r_2 + D_2r_1$. Therefore, we have $S^*(D) = \frac{\beta^2 - \sqrt{\beta^2 - 4\alpha\gamma}}{2\alpha}$.

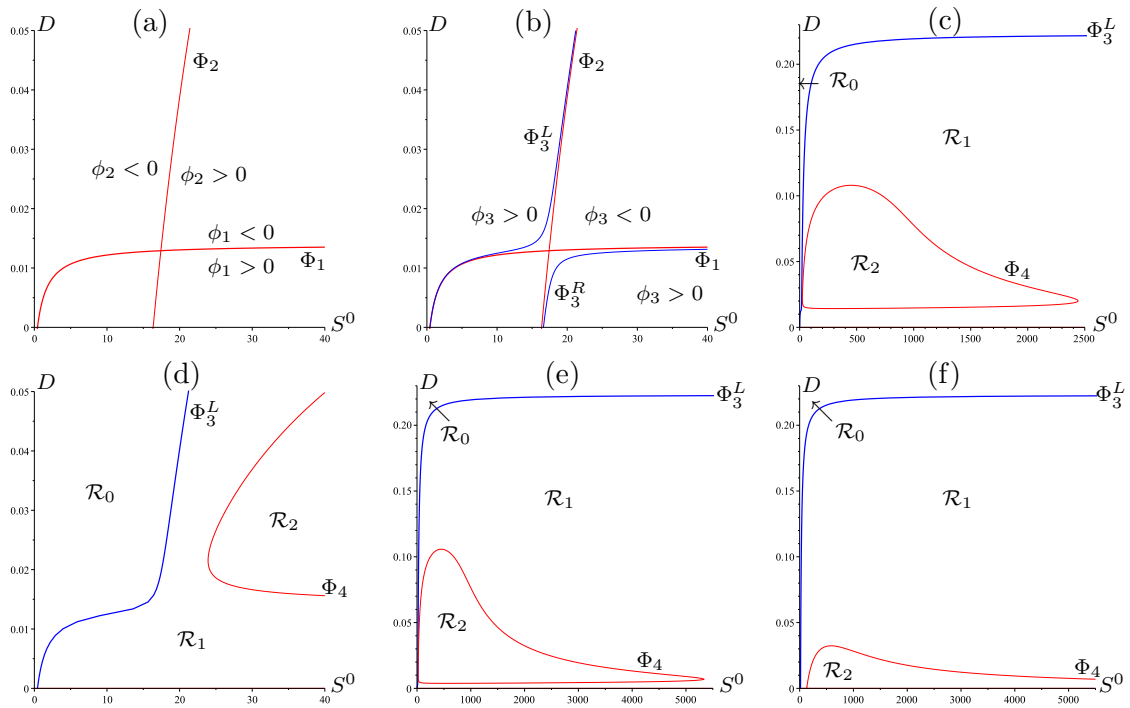

Figure 2. *(a,b) The curves Φ_i (in red), the curve $\Phi_3 = \Phi_3^L \cup \Phi_3^R$ (in blue) and the signs of ϕ_1, ϕ_2 and ϕ_3. (c,d,e,f) Operating diagram of (1.3). The asymptotic behaviour of (1.3) in the regions $\mathcal{R}_0$, $\mathcal{R}_1$ and $\mathcal{R}_2$ is given in Table 3. Biological parameter values are given in Table 4.*

4.2. Monod growth. We show now how the theory can be applied to Monod growth functions $f_i(S) = \frac{m_i S}{K_i + S}$, $i = 1, 2$, where m_i denotes the maximum growth rate and K_i the

half-saturation constant. In this case, Φ_1 and Φ_2 curves are hyperbolas, while Φ_3 is an algebraic curve (defined by a polynomial of degree four in S^0 and D), admitting Φ_1 and Φ_2 as asymptotic curves. For the biological parameter values given in Table 4, Figure 2(a) shows the signs of ϕ_1 and ϕ_2, while Figure 2(b) shows the signs of ϕ_3. We see that the condition ($\phi_1 < 0$ and $\phi_2 < 0$ and $\phi_3 > 0$), of stability of E_0, is satisfied at the left of the component Φ_3^L of Φ_3, while the condition ($\phi_1 > 0$ or $\phi_2 > 0$ or $\phi_3 < 0$) of existence of E_1 (and instability of E_0) is satisfied at right of Φ_3^L. As with linear growth functions, the equation $\phi_3 = 0$ is quadratic, so the curve Φ_3^L has an equation that can be written explicitly. Curves Φ_3^L and Φ_4 divide the

Table 4

Values of the biological parameter ε_1 used in Fig. 2 for (1.3), with Monod growth functions $f_i(S) = \frac{m_i S}{K_i + S}$, with $m_1 = 0.02$, $m_2 = 3.87$, $K_1 = K_2 = 1$, $Y_1 = 0.056$, $Y_2 = 355$, $r_1 = 0.006$, $r_2 = 0.007$, $D_1 = D + \varepsilon_1$ and $D_2 = D + 3.64$. The last column shows I_1, defined by (2.23).

Figure	ε_1	I_1
2(a,b,c)	0	(0.0142,0.108)
2(d)	0.01	(0.0038,0.106)
2(e)	0.02	(0,0.104)
2(f)	0.4	(0, 0.032)

operating plane (S^0, D) in three regions, as shown in Figure 2(c). Numerical determination of the interval I_1 is given in Appendix A.2. Since $I_1 = (D^-, D^+)$, Φ_4 is homeomorphic to the circle by Proposition 4.1, as it is seen on the figure.

Figure 2(d,e,f) shows the operating diagrams obtained when the decay rate ε_1 of x_1 is added to the model. If $\varepsilon_1 = 0.01$, $I_1 = (D^-, D^+)$, so that Φ_4 is homeomorphic to the circle by Proposition 4.1, as it is depicted in Figure 2(d). If $\varepsilon_1 = 0.02$, or If $\varepsilon_1 = 0.4$, then $I_1 = (0, D^+)$, and hence, Φ_4 is unbounded by Proposition 4.1, as it is shown in Figure 2(e,f). The $\mathcal{R}_2$ region eventually disappears. A numerical calculation shows that if $0 \leq \varepsilon_1 < 0.01346$, then $I_1 = (D^-, D^+)$, if $0.01346 < \varepsilon_1 < 0.8173$, then $I_1 = (0, D^+)$, and if $\varepsilon_1 > 0.8173$, then $I_1 = \emptyset$.

5. Hopf bifurcations and bifurcation diagrams using MATCONT. In this section, we analyse the Hopf bifurcation occurring along the Φ_4 curve. For this purpose, we fix the values of all biological parameters and the value of the operating parameter D and we numerically construct the one-parameter bifurcation diagram, where S^0 is considered as a bifurcation parameter. We use MATCONT [6], which is a MATLAB package for numerical continuation and bifurcation analysis of ODE systems. MATCONT provides numerous features allowing us to compute curves of equilibria and limit cycles as well as their local asymptotic behaviours and bifurcations, such as Branch Points of equilibria (BP), transcritical bifurcations, Hopf points (H), and limit points of cycles (LPC).

5.1. A unique limit cycle appears when E_1 is unstable. We consider linear growth rates with the biological parameter values used in Figure 1(c) and $D = 1$. The one-parameter bifurcation diagram in S^0, for fixed $D = 1$, corresponds to the horizontal line $D = 1$ in the operating diagram shown in Figure 1(c). Hence, there exists a critical value σ_1 of S^0, corresponding to the intersection of the horizontal line $D = 1$ with the Φ_3^L curve, and two other critical values σ_2 and σ_3 of S^0, corresponding to the intersection of the horizontal line $D = 1$ with the Φ_4 curve. Figure 3 shows a transcritical bifurcation (BP) at $S^0 = \sigma_1$ in

which the stability of E_0 is transferred to E_1 which emerges stable into the interior of positive cone as S^0 crosses σ_1. This bifurcation corresponds to the passage from the region $\mathcal{R}_0$ to $\mathcal{R}_1$ through the curve Φ_3^L. After that, when S^0 crosses the value σ_2, the positive equilibrium loses its stability and recovers it only when $S^0 > \sigma_3$. These bifurcations correspond to the passage from the region $\mathcal{R}_1$ to $\mathcal{R}_2$ through Φ_4, and the passage from the region $\mathcal{R}_2$ to $\mathcal{R}_1$ through Φ_4 curve, respectively.

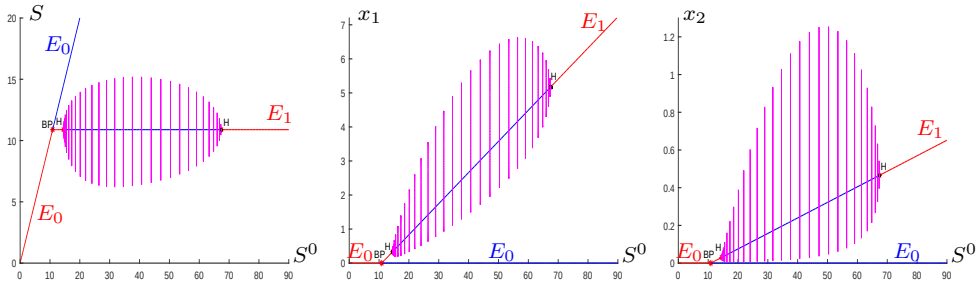

Figure 3. *Bifurcation diagram, corresponding to the case $D = 1$ of Figure 1(c), showing the equilibria and limit cycles as functions of S^0. The bifurcation values of S^0 are given in Table 5.*

Table 5

Existence and stability of the limit cycles and equilibria shown in Figure 3. The last column gives the corresponding region of Figure 1(c) and the nature of the bifurcations occurring at the critical values σ_i, as well as the first Lyapunov coefficient l_1 at Hopf points.

S^0	E_0	E_1	Cycle	Region & Bifurcation
$(0, \sigma_1)$	S			$\mathcal{R}_0$
$\sigma_1 \approx 10.889$				BP ($E_0 = E_1$)
(σ_1, σ_2)	U	S		$\mathcal{R}_1$
$\sigma_2 \approx 14.544$				Hopf ($l_1 \approx -4.720 \times 10^{-2}$)
(σ_2, σ_3)	U	U	S	$\mathcal{R}_2$
$\sigma_3 \approx 67.386$				Hopf ($l_1 \approx -9.502 \times 10^{-3}$)
$(\sigma_3, +\infty)$	U	S		$\mathcal{R}_1$

Remark 5.1. In all the figures showing bifurcation diagrams, stable (resp. unstable) equilibria or limit cycles are plotted in red or magenta (resp. blue or cyan). BP, H, and LPC denote branch points, Hopf bifurcations, and limit points of cycles, respectively.

As expected in Remark 4.2, the numerical bifurcation diagram generated using MATCONT confirms the occurrence of Hopf bifurcations at σ_2 and σ_3, as illustrated in Figure 3. Specifically, the figure shows that a first *supercritical Hopf bifurcation* (denoted by H) occurs at σ_2, with the destabilization of the positive equilibrium E_1. The first Lyapunov coefficient at this point is negative (see Table 5), indicating that the emerging periodic orbits are stable. This Hopf point serves as the starting point for the continuation of limit cycles. As S^0 increases, the diameter of the limit cycle initially grows, then shrinks until the cycle disappears via a second supercritical Hopf bifurcation at σ_3, where the equilibrium E_1 regains stability. Again, the first Lyapunov coefficient is negative, implying that periodic orbits are born stable when S^0 decreases and crosses σ_3. The type of bifurcations, their critical values, the sign of

the Lyapunov coefficients, and the corresponding asymptotic behaviour of (1.3) as a function of S^0 are summarized in Table 5.

Remark 5.2. All the bifurcation diagrams constructed using MATCONT indicate that when $D \in I_1$, the bifurcation diagram with S^0 as the bifurcation parameter is qualitatively similar to the one obtained for $D = 1$, as shown in Figure 3 and Table 5. In particular, a single stable limit cycle appears, grows, and then disappears. As a consequence, the numerical operating diagram of the system, computed using MATCONT, is the one shown in Table 6.

Table 6

Existence and stability of the equilibria and limit cycle of system (1.3) in the regions $\mathcal{R}_0$, $\mathcal{R}_1$, and $\mathcal{R}_2$ of the operating diagram shown in Figure 1(c).

Region	E_0	E_1	Cycle
$\mathcal{R}_0$	S		
$\mathcal{R}_1$	U	S	
$\mathcal{R}_2$	U	U	S

5.2. Multiplicity of limit cycles. In this section, we present the numerical operating diagrams obtained using MATCONT, corresponding to the theoretical operating diagram shown in Figure 2. As in the previously discussed example, the critical curves Φ_3^L and Φ_4, corresponding to transcritical and Hopf bifurcations, respectively, are detected. The novelty lies in the emergence of multiple limit cycles and LPC (Limit Point of Cycles) curves, which are not predicted by the theoretical operating diagram, since this diagram is based solely on conditions for the existence and stability of the system's equilibria.

5.2.1. Numerical operating diagram corresponding to Figure 2(c). We begin with the construction of the bifurcation diagram corresponding to Monod growth rates and the biological parameter values used in Figure 2(c), where $D = 0.04$, and S^0 is the free parameter. Therefore, the one-parameter bifurcation diagram corresponds to the horizontal line $D = 0.04$ of the operating diagram shown in Figure 2(c). There exist three critical values corresponding to the intersections of this horizontal line with the curves Φ_3^L and Φ_4, at which transcritical and Hopf bifurcations occur. What is new in this second example is the occurrence of two other bifurcations corresponding to LPC. As S^0 increases, MATCONT detects a BP bifurcation at the critical value σ_1 where the E_0 and E_1 exchange their stability; see Figure 4(a,b).

Starting from the BP bifurcation and increasing S^0, a supercritical Hopf (H) bifurcation occurs at $S^0 = \sigma_2$, where the positive equilibrium E_1 loses stability and a limit cycle, denoted C_1, emerges (see Figure 4(b)). The first Lyapunov coefficient at this Hopf point is negative, indicating that the periodic orbits are born stable (see Table 7). This Hopf point is used as a starting point for the continuation of the limit cycle. As S^0 increases, the amplitude of the limit cycle C_1 increases until it disappears at σ_5 via a saddle-node bifurcation, where the stable limit cycle C_1 and an unstable limit cycle C_2 collide and annihilate each other (see Figure 4(d)). Now, as S^0 decreases and the continuation is followed from the LPC bifurcation, the amplitude of the unstable limit cycle C_2 decreases until it collides with another stable limit cycle C_3 at a second LPC bifurcation point σ_3 (see Figure 4(c)). Finally, as S^0 increases and

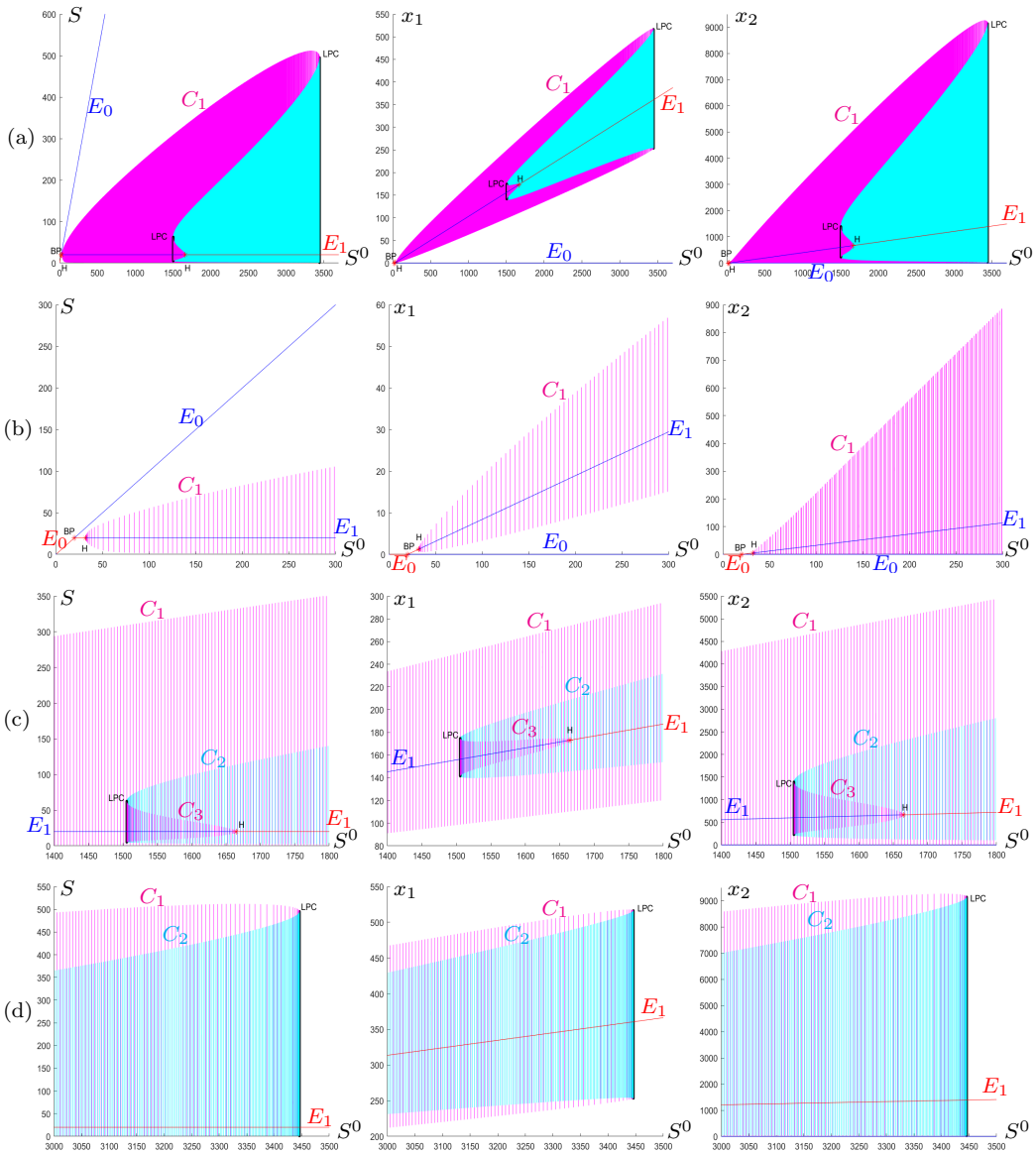

Figure 4. *(a) Bifurcation diagram corresponding to the case $D = 0.04$ from Figure 2(c), showing equilibria and limit cycles as functions of S^0. (b) Enlargement showing the BP and the first (supercritical) Hopf bifurcations. (c) Enlargement showing the first LPC and the second (supercritical) Hopf bifurcations. (d) Enlargement showing the second LPC bifurcation. The bifurcation values of S^0 are given in Table 7.*

continuation is followed from the LPC bifurcation, the stable limit cycle C_3 collapses onto the positive equilibrium E_1, which becomes stable from σ_4 via a supercritical Hopf bifurcation, since the first Lyapunov coefficient is negative (see Table 7).

When $S^0 \in (\sigma_3, \sigma_4)$, the system exhibits bistability between two stable limit cycles, C_1 and C_3, whose basins of attraction are separated by the two-dimensional stable manifold of the unstable limit cycle C_2. However, when $S^0 \in (\sigma_4, \sigma_5)$, the system displays bistability between

Table 7

Existence and stability of the limit cycles and equilibria shown in Figure 4. The last column indicates the corresponding region in Figure 5, as well as the type of bifurcations occurring at the critical values σ_i, and the first Lyapunov coefficient l_1 at the Hopf points.

S^0	E_0	E_1	C_1	C_2	C_3	Region & Bifurcation
$(0, \sigma_1)$	S					$\mathcal{R}_0$
$\sigma_1 \approx 19.969$						BP ($E_0 = E_1$)
(σ_1, σ_2)	U	S				$\mathcal{R}_1$
$\sigma_2 \approx 31.988$						Hopf ($l_1 \approx -4.482 \times 10^{-5}$)
(σ_2, σ_3)	U	U	S			$\mathcal{R}_2$
$\sigma_3 \approx 1505.540$						LPC ($C_2 = C_3$)
(σ_3, σ_4)	U	U	S	U	S	$\mathcal{R}_2^b$
$\sigma_4 \approx 1664.577$						Hopf ($l_1 \approx -1.226 \times 10^{-7}$)
(σ_4, σ_5)	U	S	S	U		$\mathcal{R}_1^b$
$\sigma_5 \approx 3445.826$						LPC ($C_1 = C_2$)
$(\sigma_5, +\infty)$	U	S				$\mathcal{R}_1$

the stable limit cycle C_1 and the positive equilibrium E_1. Table 7 summarizes the types of bifurcations, their critical values, the associated Lyapunov coefficient, and the asymptotic behaviour of (1.3) as a function of S^0.

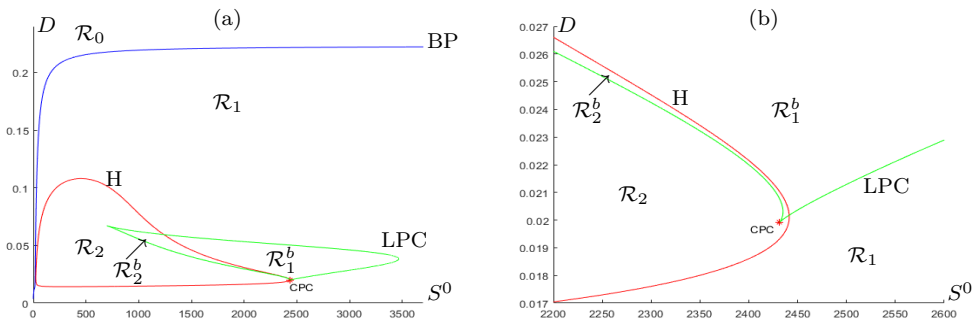

Figure 5. *(a) Operating diagram of (1.3) for the parameter values used in Figure 2(c). (b) Enlargement near the CPC bifurcation, occurring at $(S^0, D) \approx (2431.509, 0.199)$, which corresponds to the intersection point of two LPC curves. The asymptotic behaviour of (1.3) in regions $\mathcal{R}_0$, $\mathcal{R}_1$, $\mathcal{R}_1^b$, $\mathcal{R}_2$, and $\mathcal{R}_2^b$ is given in Table 8.*

Now, we use MATCONT to construct the operating diagram. To this end, we start from the BP bifurcation at $S^0 = \sigma_1$ in the one-parameter bifurcation diagram of Figure 4, corresponding to $D = 0.04$. This yields the BP curve (in blue), which coincides with the curve Φ_3^L in the operating diagram of Figure 2(c). Next, starting from the Hopf bifurcation at $S^0 = \sigma_2$ (or equivalently at $S^0 = \sigma_4$), we obtain the Hopf (H) curve (in red), which is the same as the Φ_4 curve in the operating diagram of Figure 2(c). Finally, starting from the LPC bifurcation at $S^0 = \sigma_3$ (or equivalently at $S^0 = \sigma_5$), we obtain the LPC curve (in green), which is new and was not detected in Figure 2(c) (see Figure 5(a)). In Figure 5(b), we show an enlargement near the cusp point of cycles (CPC), located on the LPC curve, where three limit cycles coincide. The figure shows that the left branch of the LPC curve lies to the left of the Hopf curve.

Table 8

Existence and stability of limit cycles and equilibria of system (1.3) in the regions $\mathcal{R}_0$, $\mathcal{R}_1$, $\mathcal{R}_1^b$, $\mathcal{R}_2$, and $\mathcal{R}_2^b$ of the operating diagrams shown in Figure 5 ($\varepsilon_1 = 0$), Figure 6 ($\varepsilon_1 = 0.01$), Figure 8 ($\varepsilon_1 = 0.02$), and Figure 10 ($\varepsilon_1 = 0.4$). The region $\mathcal{R}_1^b$ [resp. $\mathcal{R}_2^b$] exhibits bistability between a stable limit cycle and the equilibrium E_1 [resp. between two stable limit cycles].

Region	E_0	E_1	Limit cycles
$\mathcal{R}_0$	S		
$\mathcal{R}_1$	U	S	
$\mathcal{R}_1^b$	U	S	Two cycles (one stable and one unstable)
$\mathcal{R}_2$	U	U	One stable cycle
$\mathcal{R}_2^b$	U	U	Three cycles (two stable and one unstable)

The LPC curve defines two subregions, denoted $\mathcal{R}_1^b$ and $\mathcal{R}_2^b$ of the regions $\mathcal{R}_1$ and $\mathcal{R}_2$, respectively. In these subregions, the system exhibits multiple limit cycles and consequently displays bistable behaviour. In $\mathcal{R}_1^b$, both a stable limit cycle and the equilibrium point E_1 are stable. In $\mathcal{R}_2^b$, two stable limit cycles coexist, while E_1 is unstable.

The asymptotic behaviour of system (1.3) across the different regions of the operating diagram is summarized in Table 8. This behaviour should be compared with that described in Table 6, where the system admits a unique limit cycle. Illustrations of the asymptotic behaviour in the various regions of the operating diagram shown in Figure 5 are provided in Appendix B, using bifurcation diagrams with S^0 as the free parameter and several fixed values of D.

5.2.2. Numerical operating diagram corresponding to Figure 2(d). Using the same methodology as before, we construct the numerical operating diagram with MATCONT; see Figure 6. We recover the BP curve (in blue), which corresponds to the curve Φ_3^L in the operating diagram of Figure 2(d), and the Hopf (H) bifurcation curve (in red), which matches the Φ_4 curve in the same diagram. In addition, we detect a new curve, the LPC curve (in green), which was not observed in Figure 2(d). This curve defines two subregions, denoted $\mathcal{R}_1^b$ and $\mathcal{R}_2^b$ of the regions $\mathcal{R}_1$ and $\mathcal{R}_2$, respectively. In these subregions, the system exhibits multiple limit cycles and consequently displays bistable behaviour. The asymptotic behaviour of system (1.3) in the various regions of the operating diagram is summarized in Table 8.

In addition to the CPC point, MATCONT detects two new two-parameter bifurcations in the operating diagram of Figure 6, corresponding to the intersections of the Hopf (H) and Limit Point of Cycles (LPC) curves. These are identified as Generalized Hopf (GH) bifurcation points. Crossing the Hopf curve between the two GH points leads to a subcritical Hopf bifurcation, whereas crossing it on either side of the GH points results in a supercritical Hopf bifurcation.

The occurrence of a subcritical Hopf bifurcation is illustrated by the one-parameter bifurcation diagram where S^0 is the free parameter and D is fixed at $D = 0.0105$ (see Figure 7). This figure displays the equilibria and limit cycles as functions of S^0. In this case, the horizontal line $D = 0.0105$ intersects the Hopf (H) curve between the two Generalized Hopf (GH) points (see Figure 6). First, a BP bifurcation occurs at $S^0 = \sigma_1$, where equilibria E_0 and E_1 exchange stability. As S^0 increases, a supercritical Hopf bifurcation occurs at $S^0 = \sigma_2$,

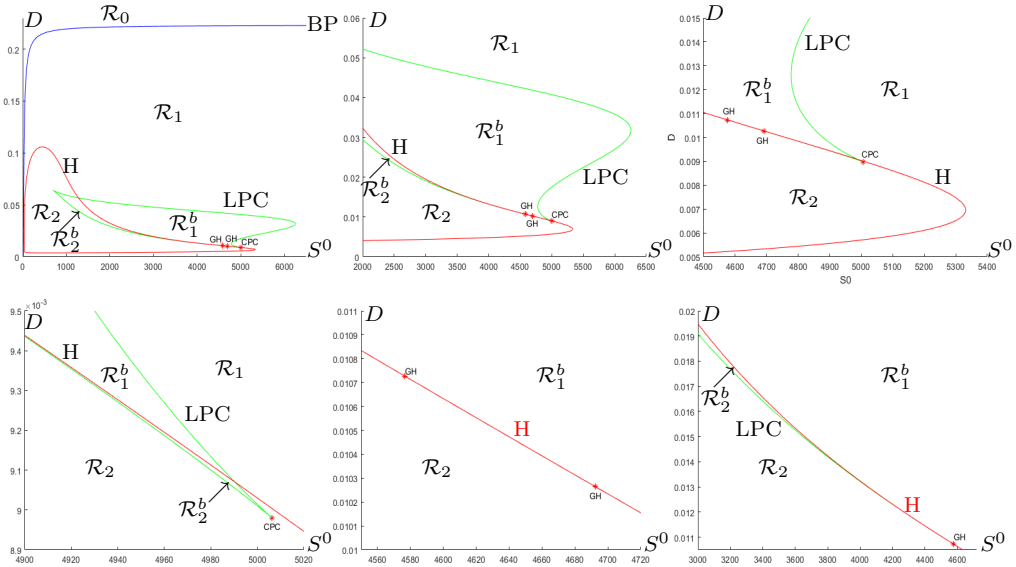

Figure 6. *Operating diagram of system (1.3) for the parameter values used in Figure 2(d), including zoomed views near the CPC point, located at* $(S^0, D^0) \approx (5006.308,\ 8.980 \times 10^{-3})$*, and two Generalized Hopf (GH) points, located at* $(S^0, D^0) \approx (4576.480,\ 0.010728)$ *and* $(S^0, D^0) \approx (4692.390,\ 0.010264)$*. The asymptotic behaviour of system (1.3) in the regions* $\mathcal{R}_0$*,* $\mathcal{R}_1$*,* $\mathcal{R}_1^b$*,* $\mathcal{R}_2$*, and* $\mathcal{R}_2^b$ *is summarized in Table 8.*

Table 9

Existence and stability of the limit cycles and equilibria depicted in Figure 7. The last column indicates the corresponding region in Figure 6, along with the nature of the bifurcations occurring at the critical values σ_i*, and the value of the first Lyapunov coefficient* l_1 *at the Hopf bifurcation points.*

S^0	E_0	E_1	C_1	C_2	Region & Bifurcation
$(0, \sigma_1)$	S				$\mathcal{R}_0$
$\sigma_1 \approx 16.752$					BP $(E_0 = E_1)$
(σ_1, σ_2)	U	S			$\mathcal{R}_1$
$\sigma_2 \approx 20.553$					Hopf $(l_1 \approx -1.015 \times 10^{-3})$
(σ_2, σ_3)	U	U	S		$\mathcal{R}_2$
$\sigma_3 \approx 4633.239$					Hopf $(l_1 \approx 6.690 \times 10^{-10})$
(σ_3, σ_4)	U	S	S	U	$\mathcal{R}_1^b$
$\sigma_4 \approx 4840.055$					LPC $(C_1 = C_2)$
$(\sigma_4, +\infty)$	U	S			$\mathcal{R}_1$

where E_1 loses stability and a stable limit cycle C_1 emerges, as confirmed by a negative first Lyapunov coefficient (see Table 9). Further increasing S^0 leads to the disappearance of the stable cycle C_1 at $S^0 = \sigma_4$ through a Limit Point of Cycles (LPC) bifurcation. When S^0 decreases from this point, an unstable limit cycle C_2 emerges (see Figure 7). The amplitude of C_2 gradually decreases until it collapses onto the positive equilibrium E_1 at $S^0 = \sigma_3$ via a subcritical Hopf bifurcation, as the first Lyapunov coefficient is positive (see Table 9). Conversely, continuing from σ_3 by increasing S^0 leads to the stabilization of E_1.

Therefore, when $S^0 \in (\sigma_3, \sigma_4)$, the system exhibits bistability between the stable limit cycle C_1 and the positive equilibrium E_1. This behaviour corresponds to region $\mathcal{R}_1^b$ in Figure 6. The

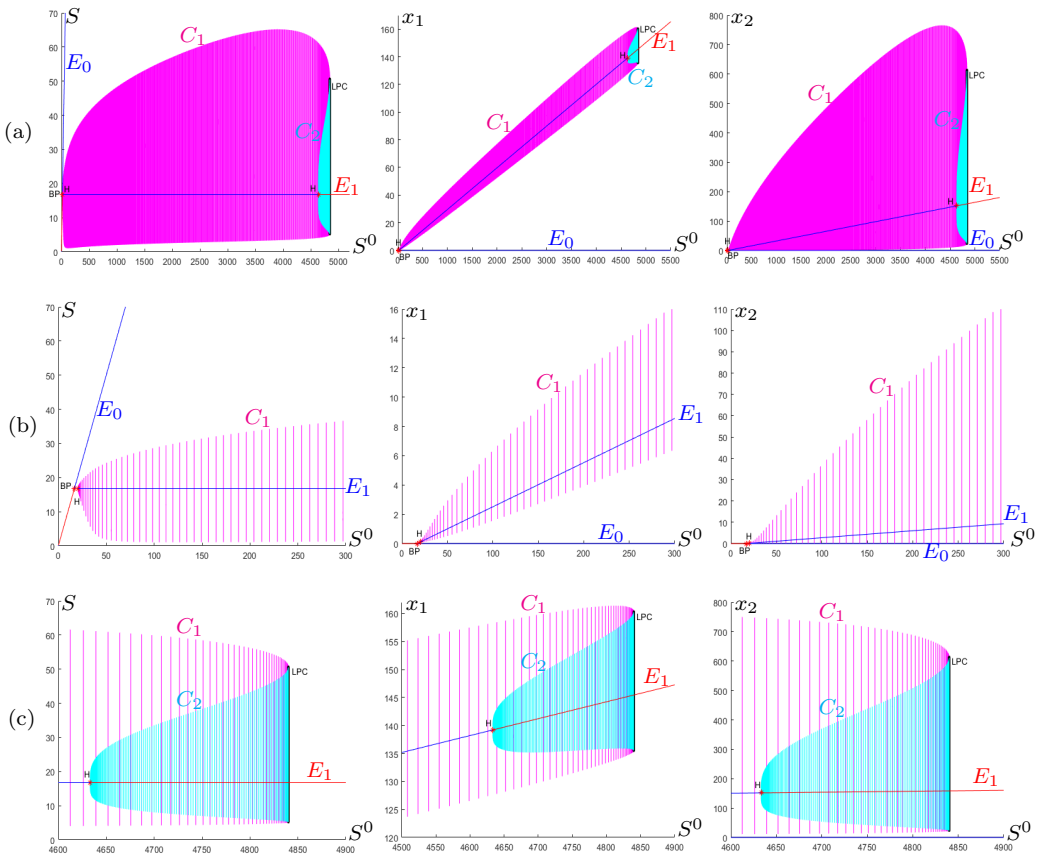

Figure 7. *(a) Bifurcation diagram corresponding to the case $D = 0.0105$ from Figure 2(d), showing the equilibria and limit cycles as functions of S^0. (b) Zoomed view highlighting the BP bifurcation and the first (supercritical) Hopf bifurcation. (c) Zoomed view showing the second (subcritical) Hopf bifurcation and the LPC bifurcation. The corresponding bifurcation values of S^0 are listed in Table 9.*

asymptotic dynamics in the various regions of the operating diagram shown in Figure 6 are further illustrated in Appendix C using bifurcation diagrams where S^0 is the free parameter and D is fixed at several values.

5.2.3. Numerical operating diagram corresponding to Figure 2(e). Using the same methodology as before, we construct the numerical operating diagram using MATCONT (see Figure 8). The resulting diagram includes the BP curve (in blue) and the Hopf (H) curve (in red), which correspond to the Φ_3^L and Φ_4 curves, respectively, in the operating diagram of Figure 2(e). In addition, a new Limit Point of Cycles (LPC) curve (in green) is detected, which was not visible in Figure 2(e). This LPC curve defines the sub-regions $\mathcal{R}_1^b$ and $\mathcal{R}_2^b$ within regions $\mathcal{R}_1$ and $\mathcal{R}_2$, respectively, where multiple limit cycles exist and bistability occurs. The asymptotic behaviour of system (1.3) in the different regions of the operating diagram is summarized in Table 8.

In addition to the Cusp Point of Cycles (CPC), MATCONT also detects a Generalized Hopf (GH) bifurcation point, located at the intersection of the LPC and H curves. Crossing the H curve to the right of the GH point leads to a subcritical Hopf bifurcation, whereas

crossing it to the left results in a supercritical Hopf bifurcation.

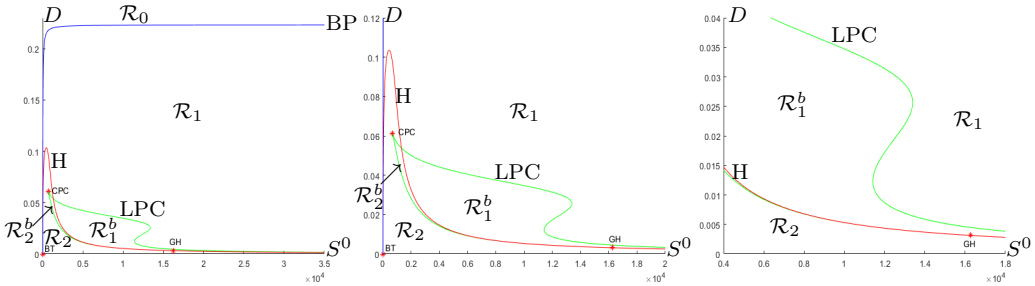

Figure 8. *Operating diagram of system (1.3) for the parameter values used in Figure 2(e), including two enlargements near the Cusp Point of Cycles (CPC), located at* $(S^0, D) \approx (693.581, 6.417 \times 10^{-2})$*, and the Generalized Hopf (GH) point, located at* $(S^0, D) \approx (16251.254, 0.003140)$*. The asymptotic behaviour of system (1.3) in the regions* $\mathcal{R}_0$*,* $\mathcal{R}_1$*,* $\mathcal{R}_1^b$*,* $\mathcal{R}_2$ *and* $\mathcal{R}_2^b$ *is summarized in Table 8.*

Table 10

Existence and stability of the limit cycles and equilibria shown in Figure 9. The last column indicates the corresponding region in Figure 8, the nature of the bifurcations occurring at the critical values σ_i*, and the sign of the first Lyapunov coefficient* l_1 *at the Hopf bifurcation points.*

S^0	E_0	E_1	C_1	C_2	C_3	Region & Bifurcation
$(0, \sigma_1)$	S					$\mathcal{R}_0$
$\sigma_1 \approx 22.081$						BP ($E_0 = E_1$)
(σ_1, σ_2)	U	S				$\mathcal{R}_1$
$\sigma_2 \approx 53.928$						Hopf ($l_1 \approx -2.290 \times 10^{-6}$)
(σ_2, σ_3)	U	U	S			$\mathcal{R}_2$
$\sigma_3 \approx 842.335$						LPC ($C_2 = C_3$)
(σ_3, σ_4)	U	U	S	U	S	$\mathcal{R}_2^b$
$\sigma_4 \approx 1059.831$						LPC ($C_1 = C_2$)
(σ_4, σ_5)	U	U			S	$\mathcal{R}_2$
$\sigma_5 \approx 1286.071$						Hopf ($l_1 \approx -8.294 \times 10^{-8}$)
$(\sigma_5, +\infty)$	U	S				$\mathcal{R}_1$

We illustrate the asymptotic behaviour in the regions of the operating diagram shown in Figure 8 by constructing a bifurcation diagram with S^0 as the free parameter and for a fixed value of $D = 0.056$; see Figure 9. This corresponds to the horizontal line $D = 0.056$ in the operating diagram of Figure 8. A BP bifurcation occurs first at $S^0 = \sigma_1$, where the equilibria E_0 and E_1 exchange stability. As S^0 increases, a supercritical Hopf (H) bifurcation occurs at $S^0 = \sigma_2$, where E_1 loses stability and a stable limit cycle C_1 emerges, since the first Lyapunov coefficient is negative (see Table 10). As S^0 continues to increase, the limit cycle C_1 disappears at σ_4 through a limit point of cycles (LPC) bifurcation. When S^0 decreases from this value, an unstable limit cycle C_2 emerges (see Figure 9). The diameter of the unstable cycle C_2 gradually decreases until it collides with a stable limit cycle C_3 at $S^0 = \sigma_3$ via a second LPC bifurcation. Then, by increasing S^0 from this point, the stable limit cycle C_3 collapses onto the positive equilibrium E_1, which regains stability through a supercritical Hopf bifurcation at σ_4, as the first Lyapunov coefficient remains negative (see Table 10).

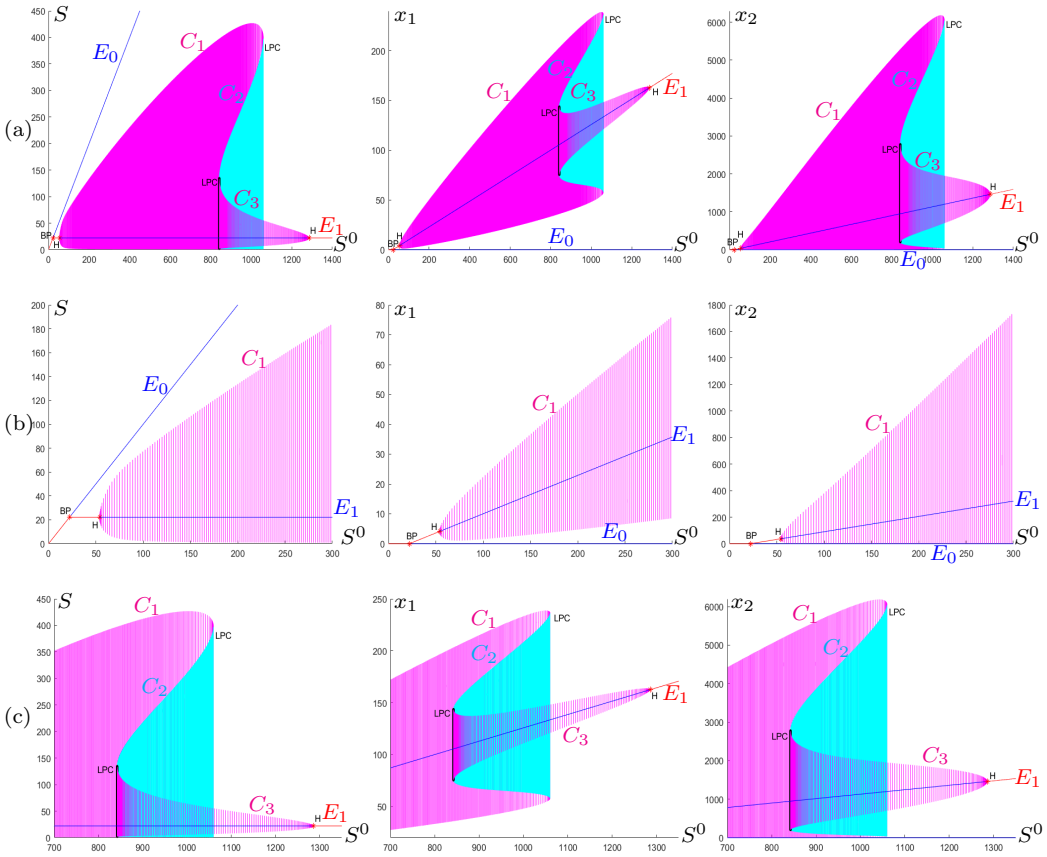

Figure 9. *(a) Bifurcation diagram corresponding to the case $D = 0.056$ from Figure 2(e), showing the equilibria and limit cycles as functions of S^0. (b) Enlargement highlighting the BP and the first (supercritical) Hopf bifurcation. (c) Enlargement showing the two LPC bifurcations and the second (supercritical) Hopf bifurcation. The bifurcation values of S^0 are listed in Table 9.*

Therefore, for $S^0 \in (\sigma_3, \sigma_4)$, the system exhibits bistability between two stable limit cycles, C_1 and C_3, whose basins of attraction are separated by the two-dimensional stable manifold of the unstable cycle C_2. This behaviour corresponds to region $\mathcal{R}_2^b$ of the operating diagram in Figure 8. The asymptotic behaviour across the various regions of the operating diagram in Figure 8 is further illustrated in Appendix D using bifurcation diagrams where S^0 is the bifurcation parameter and several values of D are considered.

5.2.4. Numerical operating diagram corresponding to Figure 2(f). Using the same methodology as in the previous cases, we construct the numerical operating diagram using MATCONT; see Figure 10. The BP curve (in blue) and the H curve (in red) correspond to the curves Φ_3^L and Φ_4 in the operating diagram of Figure 2(f), respectively. However, several numerical instabilities were encountered, which prevented us from obtaining a complete depiction of the diagram. In particular, we were unable to compute the LPC curve (in green) for very small values of D, and its behaviour near the horizontal axis remains unknown.

The LPC curve lies to the left of the H curve. Consequently, the region $\mathcal{R}_2^b$ does not exist in this case. We illustrate the asymptotic behaviour of the system in the various regions of the

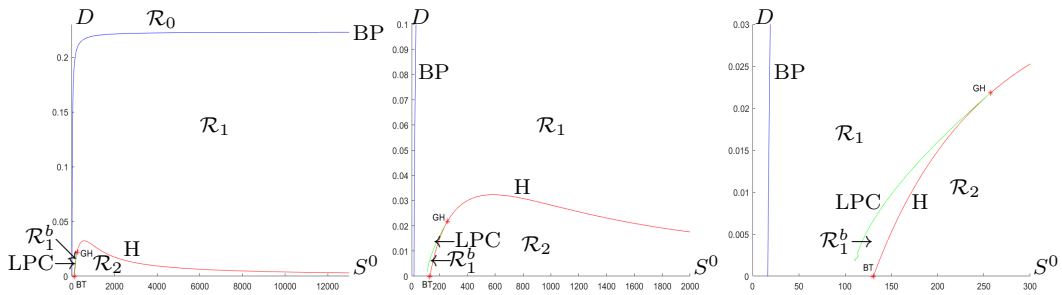

Figure 10. *Operating diagram of system (1.3) for the parameter values used in Figure 2(e), along with two zoomed-in views near the GH point, highlighting the LPC curve and the subregion $\mathcal{R}_1^b$. Note that the region $\mathcal{R}_2^b$ does not exist in this case. The asymptotic behaviour of system (1.3) in the regions $\mathcal{R}_0$, $\mathcal{R}_1$, $\mathcal{R}_1^b$, and $\mathcal{R}_2$ is summarized in Table 8.*

operating diagram shown in Figure 10 by constructing the corresponding bifurcation diagram with S^0 as the free parameter and D fixed at 0.001; see Figure 11. This figure shows the three components S, x_1, and x_2 of both equilibria and limit cycles as functions of S^0. Accordingly, the one-parameter bifurcation diagram corresponds to the horizontal line $D = 0.001$ in the operating diagram of Figure 10.

Table 11

Existence and stability of the limit cycles and equilibria shown in Figure 11. The last column indicates the corresponding region in Figure 2(f), the nature of the bifurcations occurring at the critical values σ_i, and the first Lyapunov coefficient l_1 at the Hopf points.

S^0	E_0	E_1	C_1	C_2	Region & Bifurcation
$(0, \sigma_1)$	S				$\mathcal{R}_0$
$\sigma_1 \approx 17.160$					BP ($E_0 = E_1$)
(σ_1, σ_2)	U	S			$\mathcal{R}_1$
$\sigma_2 \approx 151.734$					LPC ($C_1 = C_2$)
(σ_2, σ_3)	U	S	S	U	$\mathcal{R}_1^b$
$\sigma_3 \approx 171.699$					Hopf ($l_1 \approx 1.240 \times 10^{-7}$)
(σ_3, σ_4)	U	U	S		$\mathcal{R}_2$
$\sigma_4 \approx 3750.763$					Hopf ($l_1 \approx -6.311 \times 10^{-8}$)
$(\sigma_4, +\infty)$	U	S			$\mathcal{R}_1$

A BP bifurcation first occurs at $S^0 = \sigma_1$, involving an exchange of stability between the equilibria E_0 and E_1. As S^0 increases, a subcritical Hopf (H) bifurcation takes place at $S^0 = \sigma_3$, where E_1 loses stability. When decreasing S^0 from σ_3, an unstable limit cycle C_2 emerges, as indicated by the positive value of the first Lyapunov coefficient (see Table 11). As S^0 further decreases, the amplitude of this unstable cycle increases until it disappears via a limit point of cycles (LPC) bifurcation at $S^0 = \sigma_2$. When increasing S^0 from σ_2, a stable limit cycle C_1 emerges (see Figure 11(b-c)). The amplitude of this stable cycle initially increases and then decreases until it vanishes into the positive equilibrium E_1 at $S^0 = \sigma_4$ through a supercritical Hopf bifurcation, again confirmed by a negative first Lyapunov coefficient (see Table 11). Consequently, for $S^0 \in (\sigma_2, \sigma_3)$, the system exhibits bistability between the stable limit cycle C_1 and the positive equilibrium E_1.

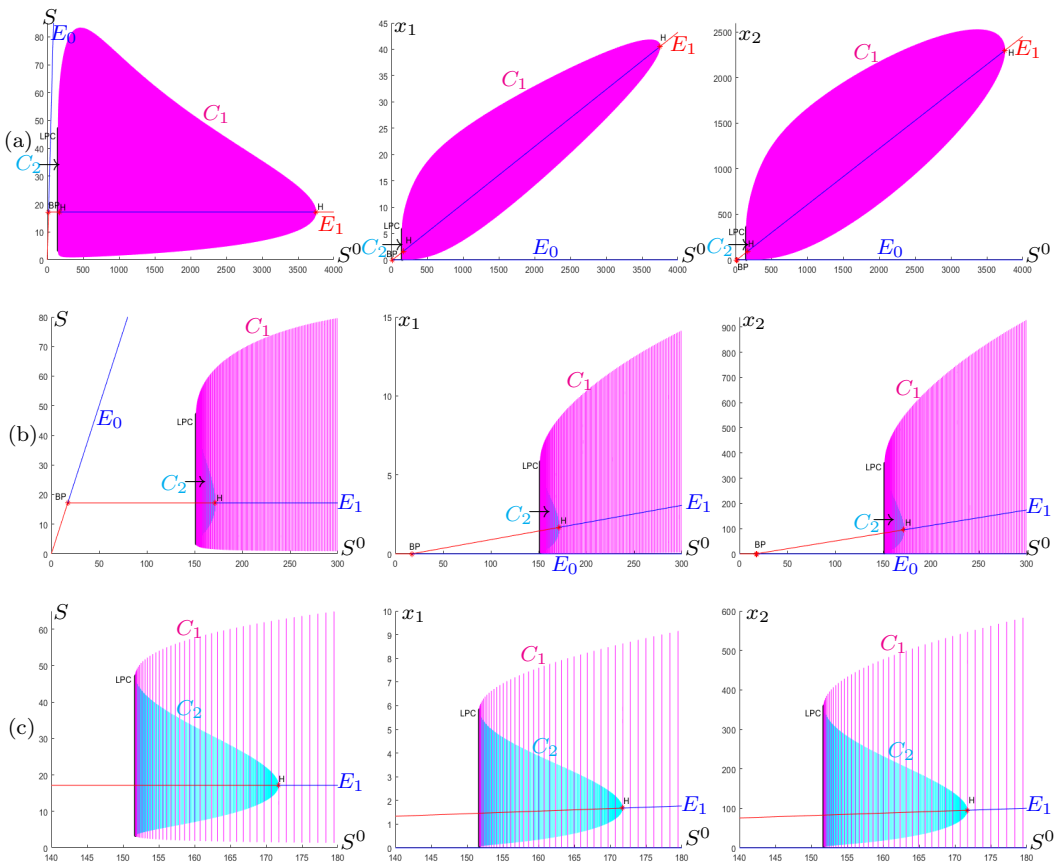

Figure 11. *(a) Bifurcation diagram corresponding to the case $D = 0.01$ from Figure 2(f), illustrating the equilibria and limit cycles as functions of S^0. (b) Enlargement highlighting the BP bifurcation. (c) Enlargement showing the LPC and the first (subcritical) Hopf bifurcations. The corresponding bifurcation values of S^0 are listed in Table 11.*

6. Conclusions.

We have described a chemostat model of competition between two populations with linear coupling between them. Unlike the classical model of competition in the chemostat, there is no competitive exclusion equilibrium, where one population dies out and the other does not. The model has only two equilibria, a total washout equilibrium and an interior coexistence equilibrium. The stability properties of each were provided. The removal rates of the populations are not equal to the dilution rate, destroying one of the basic tenets of the usual model, a conservation principle. This principle, in turn, is one of the key steps in reducing many chemostat models to a monotone dynamical system where strong convergence properties are in evidence. The study of stability requires the use of Routh-Hurwitz conditions for the three-dimensional system. The positive equilibrium can be unstable.

Two classical examples were considered in the literature. We can think of the two populations as the same population, classified by its compartment: the population could adhere to the wall (or other marked surface inserted into the medium) and could shear from the wall into the medium [23]. We can also think of the two populations as strains of a population, and model the interactions accordingly [4, 17].

These two classes of examples have been considered in the literature in particular cases where the positive equilibrium is stable as soon as it exists. These special cases correspond to fairly restrictive situations regarding the removal rates of the species and their yield coefficients. Our main contribution has been to show that this stability is no longer guaranteed when these assumptions are weakened.

Unlike the case considered in [4, 17], where the positive equilibrium is stable when $Y_1 = Y_2$ and $D_1 = D_2 = D$, Example 3.1 shows that the coexistence equilibrium is not necessarily stable if we assume that $Y_1 \neq Y_2$ and $D_1 = D_2 = D$. Example 3.2 shows that the coexistence equilibrium is not necessarily stable if we assume that $Y_1 = Y_2$ and $D_1 \neq D$, $D_2 \neq D$. These situations are very important from a biological point of view, given the importance of yield concepts and the role of microbial species mortality.

Similarly, unlike the case considered in [23], where the positive equilibrium is stable when $Y_1 = Y_2$ and $D_1 = D$, $D_2 = 0$, Example 3.3 shows that the coexistence equilibrium is not necessarily stable if we assume that $Y_1 \neq Y_2$ and $D_1 = D$, $D_2 = 0$. Example 3.4 shows that the coexistence equilibrium is not necessarily stable if we assume that $Y_1 = Y_2$ and $D_1 \neq D$, $D_2 \neq 0$.

Moreover, in our approach, strict monotonicity is not required for the two growth functions, or for at least one of them. It is only required that $f_1(0) = f_2(0) = 0$, $f_1' \geq 0$, $f_2' \geq 0$ and for every $S > 0$, $f_1'(S) > 0$ or $f_2'(S) > 0$.

We also constructed the operating diagram describing the long-time behaviour in the chemostat depending on the operating parameters D and S^0. The operating diagram is the bifurcation diagram that shows how the system behaves when we vary the parameters D and S^0. This bifurcation diagram is very useful to understand the model from both the mathematical and biological points of view. Although this diagram was not considered in the classic monograph on the chemostat of Smith and Waltman [29], its importance was clearly recognized. Indeed, in the last lines of the last chapter - devoted to open problems in the chemostat - it is stated that the operating diagram is probably the most useful answer for discussing the behaviour of the model in relation to the parameters, see [29, p. 252]. The operating diagram is constructed in the recent book on the mathematical theory of the chemostat [13]. It is often constructed both in the biological literature and in the mathematical literature, see [3, 7, 10, 20, 21, 26, 27] and the references therein.

Another model of mutation in the chemostat is given by the following system

$$\begin{aligned} x_1' &= [f_1(S) - D_1]x_1 - \beta_1 f_1(S)x_1 + \beta_2 f_2(S)x_2, \\ x_2' &= [f_2(S) - D_2]x_2 + \beta_1 f_1(S)x_1 - \beta_2 f_2(S)x_2, \\ S' &= (S^0 - S)D - \tfrac{1}{Y_1} f_1(S)x_1 - \tfrac{1}{Y_2} f_2(S)x_2, \end{aligned} \tag{6.1}$$

where $0 \leq \beta_i \leq 1$, $i = 1, 2$. We can think of x_1 as the density of a population which has a mutant of density x_2. Parameter β_i represents the fraction of nutrient consumption devoted to mutant production. Therefore, $(1 - \beta_i)f_i(S)x_i$ represents the rate of growth of species x_i, $i = 1, 2$, while $\beta_i f_i(S)x_i$ represents the rate of production of its mutant x_j, $j \neq i$. This system was studied in [1, 30] in the special case where $Y_1 = Y_2 = 1$ and $D_1 = D_2 = D$, and the system can be reduced to a two-dimensional one. Extending the methods and the results of this paper to model (6.1) is the aim of future work. For complements on this type of model and interesting numerical simulations, see Lobry [18].

Model (6.1) is similar to model (1.3), where the linear transfer term r_i is replaced by $\beta_i f_i(S)$, $i = 1, 2$. Note that a more general class of compartmental models, where r_i is replaced by a function $\alpha_i(S, x_1, x_2)$, $i = 1, 2$ is the model of flocculation

$$\begin{array}{rcl} S' & = & (S^0 - S)D - \frac{1}{Y_1} f_1(S)x_1 - \frac{1}{Y_2} f_2(S)x_2, \\ x_1' & = & [f_1(S) - D_1]x_1 - \alpha_1(S, x_1, x_2)x_1 + \alpha_2(S, x_1, x_2)x_2, \\ x_2' & = & [f_2(S) - D_2]x_2 + \alpha_1(S, x_1, x_2)x_1 - \alpha_2(S, x_1, x_2)x_2, \end{array} \tag{6.2}$$

where $x_1(t)$ and $x_2(t)$ denote, respectively, the concentration of the population of planktonic microorganisms and flocks of bacteria at time t. Isolated bacteria and flocks can stick together to form new flocks, with rate $\alpha_1(S, x_1, x_2)x_1$, and flocks can split and liberate isolated bacteria, with rate $\alpha_2(S, x_1, x_2)x_2$. Several forms of the attachment and detachment terms α_1 and α_2 have been considered in the literature [9, 10, 12, 24]. System (1.3) represents an interesting and new class of models of type (6.2).

Beyond the theoretical operating diagrams discussed in section 4, which delineate regions where the positive equilibrium can lose stability via Hopf bifurcations, the numerical operating diagrams constructed in section 5 uncover a much richer set of dynamical behaviors. In particular, they reveal the existence of new regions where multiple limit cycles both stable and unstable coexist, leading to complex forms of bistability. These regions of multistability, involving limit cycles, are not predicted by the theoretical DO, which focuses primarily on equilibrium bifurcations. The numerical diagrams, based on continuation methods, detect intricate bifurcation structures such as generalized Hopf (GH) points, cusp points of cycles (CPC), and multiple limit point of cycles (LPC) bifurcations, thereby providing a more complete picture of the system's potential dynamics. This illustrates the importance of combining analytical and numerical approaches for a deeper understanding of nonlinear biological models.

Finally, except in the case where $f_2 = 0$, the question of global asymptotic stability of the positive equilibrium E_1 remains an open issue. Our study reveals that the region $\mathcal{R}_1^b$, where E_1 is stable, with the presence of two limit cycles, one stable and one unstable, can be nonempty, see Figures 5, 6, 8, and 10. This indicates that global stability cannot hold universally, as the presence of such multistability scenarios precludes convergence to E_1 from all initial conditions. These findings highlight the need for further analytical investigations to characterize the global dynamics and identify parameter regimes where global stability may still hold.

Appendix A. Numerical experimentation.

A.1. Determining I_1 for the examples in Table 1. In this section, we perform numerical calculations to determine the signs of $b(D)$ and $\Delta(D)$ and deduce the interval I_1 defined by (2.23). We use the values of biological parameters given in Table 1. Plotting the curves of functions $b(D)$ and $\Delta(D)$, we see that their signs are as given in Table 12. Therefore, the interval I_1 is as shown in Table 1.

A.2. Determining I_1 for the examples in Table 4. For the Monod growth functions considered in Table 4, functions $b(D)$ and $\Delta(D)$ are defined for $D \in [0, D_0)$, where $D_0 = \frac{m_2 - r_2 - \varepsilon_2}{\alpha_2} \approx 0.223$. Hence, the curves of these functions should be constructed on this interval. Their signs are as given in Table 12. Therefore, the interval I_1 is as shown in the caption of Table 4.

Table 12

Signs of $b(D)$ and $\Delta(D)$ for the biological parameter values used in Figures 1 and 2.

Figure 1(a,b,c)

D		0.165		0.215		0.271		1.844		4.547	
$b(D)$	+	+	+	0	-	-	-	-	-	0	+
$\Delta(D)$	+	0	-	-	-	0	+	0	-	-	-

Figure 1(d)

D		0.048		0.168		1.254	
$b(D)$	-	-	-	0	+	+	+
$\Delta(D)$	+	0	-	-	-	0	+

Figure 1(e)

D		0.029		0.035		0.039		0.839		1.645		28.197	
$b(D)$	+	+	+	0	-	-	-	-	-	0	+	+	+
$\Delta(D)$	+	0	-	-	-	0	+	0	-	-	-	0	+

Figure 1(f)

D		0.049		0.154		0.470	
$b(D)$	-	-	-	0	+	+	+
$\Delta(D)$	+	0	-	-	-	0	+

Figure 2(a,b,c,d)

D		0.0131		0.0138		0.0142		0.108		0.171	
$b(D)$	+	+	+	0	-	-	-	-	-	0	+
$\Delta(D)$	+	0	-	-	-	0	+	0	-	-	-

Figure 2(e)

D		0.0033		0.0035		0.0038		0.106		0.173	
$b(D)$	+	+	+	0	-	-	-	-	-	0	+
$\Delta(D)$	+	0	-	-	-	0	+	0	-	-	-

Figure 2(f)

D		0.032		0.098	
$b(D)$	-	-	-	0	+
$\Delta(D)$	+	0	-	-	-

Appendix B. Numerical bifurcation diagrams illustrating Figure 5 ($\varepsilon_1 = 0$). In this section, we present several bifurcation diagrams for fixed values of D while varying S^0, in order to illustrate the dynamical behaviours associated with the different regions of the operating diagram shown in Figure 5 and Table 8. These diagrams were obtained using the biological parameter values from Figure 2(c).

B.1. Bifurcation diagram for $D = 0.02$. The one-parameter bifurcation diagram in S^0, for fixed $D = 0.02$, corresponds to the horizontal line $D = 0.02$ in the operating diagram shown in Figure 5. Figure 12 and Table 13 (for $D = 0.02$) reveal five critical bifurcation values $\sigma_1 < \sigma_2 < \sigma_3 < \sigma_4 < \sigma_5$, which correspond to the intersections of the line $D = 0.02$ with the BP, H, LPC, LPC, and H curves, respectively. More precisely, a transcritical bifurcation (BP) occurs at $S^0 = \sigma_1$, where stability is transferred from E_0 to E_1. As S^0 increases, a supercritical Hopf bifurcation (H) occurs at $S^0 = \sigma_2$, where E_1 destabilizes and a stable limit

Table 13

Existence and stability of the limit cycles and equilibria shown in Figures 12 to 14. The last column gives the corresponding region of Figure 5 ($\varepsilon_1 = 0$) and the nature of the bifurcations occurring at the critical values σ_i, as well as the first Lyapunov coefficient l_1 at Hopf points.

Figure 12 ($D = 0.02$)

S^0	E_0	E_1	C_1	C_2	C_3	Region & Bifurcation
$(0, \sigma_1)$	S					$\mathcal{R}_0$
$\sigma_1 \approx 17.523$						BP ($E_0 = E_1$)
(σ_1, σ_2)	U	S				$\mathcal{R}_1$
$\sigma_2 \approx 24.143$						Hopf ($l_1 \approx -6.875 \times 10^{-4}$)
(σ_2, σ_3)	U	U	S			$\mathcal{R}_2$
$\sigma_3 \approx 2432.960$						LPC ($C_2 = C_3$)
(σ_3, σ_4)	U	U	S	U	S	$\mathcal{R}_2^b$
$\sigma_4 \approx 2434.050$						LPC ($C_1 = C_2$)
(σ_4, σ_5)	U	U			S	$\mathcal{R}_2$
$\sigma_5 \approx 2441.247$						Hopf ($l_1 \approx -7.873 \times 10^{-8}$)
$(\sigma_5, +\infty)$	U	S				$\mathcal{R}_1$

Figure 13 ($D = 0.065$)

S^0	E_0	E_1	C_1	C_2	C_3	Region & Bifurcation
$(0, \sigma_1)$	S					$\mathcal{R}_0$
$\sigma_1 \approx 23.369$						BP ($E_0 = E_1$)
(σ_1, σ_2)	U	S				$\mathcal{R}_1$
$\sigma_2 \approx 59.601$						Hopf ($l_1 \approx -1.791 \times 10^{-6}$)
(σ_2, σ_3)	U	U	S			$\mathcal{R}_2$
$\sigma_3 \approx 758.485$						LPC ($C_2 = C_3$)
(σ_3, σ_4)	U	U	S	U	S	$\mathcal{R}_2^b$
$\sigma_4 \approx 789.792$						LPC ($C_1 = C_2$)
(σ_4, σ_5)	U	U			S	$\mathcal{R}_2$
$\sigma_5 \approx 1156.512$						Hopf ($l_1 \approx -8.211 \times 10^{-8}$)
$(\sigma_5, +\infty)$	U	S				$\mathcal{R}_1$

Figure 14 ($D = 0.08$)

S^0	E_0	E_1	C_1	Region & Bifurcation
$(0, \sigma_1)$	S			$\mathcal{R}_0$
$\sigma_1 \approx 25.944$				BP ($E_0 = E_1$)
(σ_1, σ_2)	U	S		$\mathcal{R}_1$
$\sigma_2 \approx 95.291$				Hopf ($l_1 \approx -3.336 \times 10^{-7}$)
(σ_2, σ_3)	U	U	S	$\mathcal{R}_2$
$\sigma_3 \approx 974.186$				Hopf ($l_1 \approx -6.190 \times 10^{-8}$)
$(\sigma_3, +\infty)$	U	S		$\mathcal{R}_1$

cycle C_1 emerges, as the first Lyapunov coefficient is negative (see Table 13, case $D = 0.02$). Upon further increase of S^0, the limit cycle C_1 disappears at σ_4 through an LPC bifurcation. When S^0 decreases from σ_4, an unstable limit cycle C_2 is created (see Figure 12). As S^0 continues to decrease, the diameter of C_2 shrinks until it collides with a stable limit cycle C_3 at σ_3 in a second LPC bifurcation. Beyond this point, as S^0 increases from σ_3, the stable cycle C_3 persists and eventually collapses onto the equilibrium E_1, which regains stability at σ_5 via a supercritical Hopf bifurcation (again with a negative first Lyapunov coefficient).

Thus, for $S^0 \in (\sigma_3, \sigma_4)$, the system exhibits bistability between two stable limit cycles, C_1

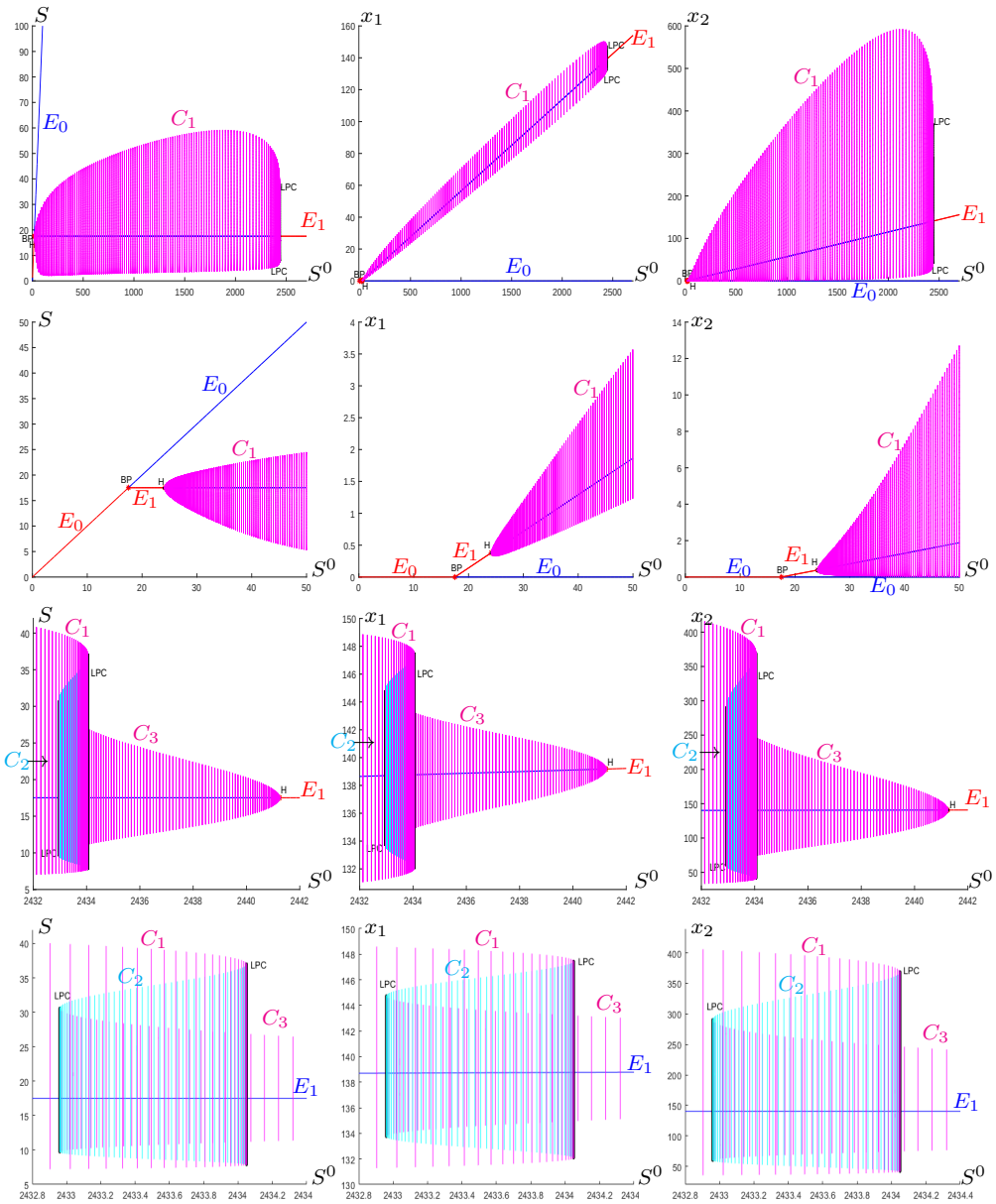

Figure 12. *Bifurcation diagram, corresponding to the case* $D = 0.02$ *of Figure 5, showing the equilibria and limit cycles as functions of* S^0. *The bifurcation values of* S^0 *are given in Table 13.*

and C_3. Their basins of attraction are separated by the two-dimensional stable manifold of the intermediate unstable limit cycle C_2. This dynamic scenario corresponds to region $\mathcal{R}_2^b$ in Figure 5.

B.2. Bifurcation diagram for $D = 0.065$. The one-parameter bifurcation diagram in S^0, for fixed $D = 0.065$, corresponds to the horizontal line $D = 0.065$ in the operating diagram shown in Figure 5. Figure 13 and Table 13 (for $D = 0.065$) display five bifurcation values,

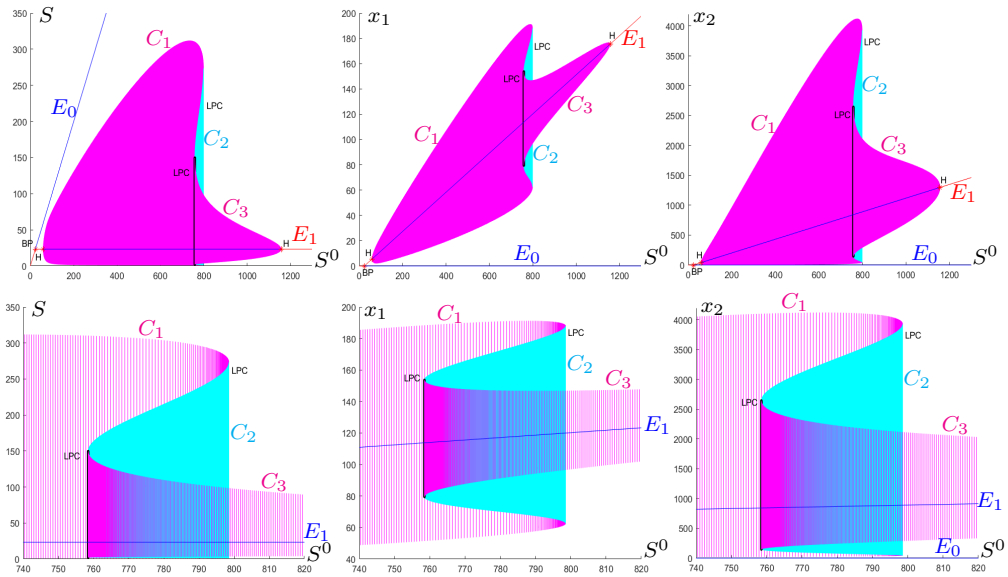

Figure 13. *Bifurcation diagram corresponding to the case $D = 0.065$ in Figure 5, showing equilibria and limit cycles as functions of S^0. The bifurcation values of S^0 associated with this diagram are listed in Table 13.*

$\sigma_1 < \sigma_2 < \sigma_3 < \sigma_4 < \sigma_5$, corresponding to the intersections of the line $D = 0.065$ with the BP, H, LPC, LPC, and H curves, respectively. The bifurcation diagram shown in Figure 13 is constructed in the same way as described in Appendix B.1, and the detailed description is therefore omitted here.

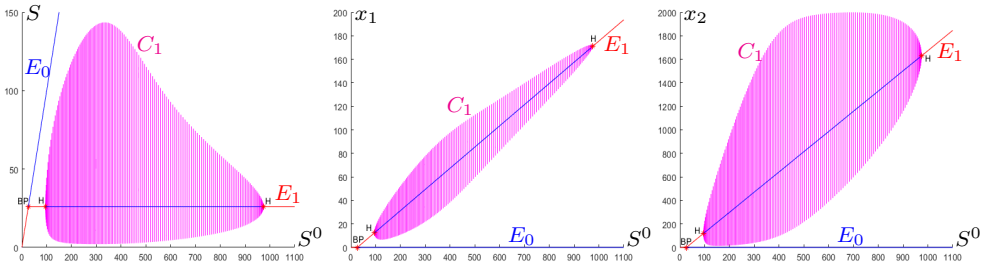

Figure 14. *Bifurcation diagram corresponding to the case $D = 0.08$ in Figure 5, showing equilibria and limit cycles as functions of S^0. The corresponding bifurcation values of S^0 are listed in Table 13.*

B.3. Bifurcation diagram for $D = 0.08$. The one-parameter bifurcation diagram in S^0, for fixed $D = 0.08$, corresponds to the horizontal line $D = 0.08$ in the operating diagram shown in Figure 5. Figure 14 and Table 13 (for $D = 0.08$) indicate three bifurcation values, $\sigma_1 < \sigma_2 < \sigma_3$, corresponding to the intersections of the line $D = 0.08$ with the BP, H, and H curves, respectively. The construction of the bifurcation diagram in Figure 14 follows the same procedure as described in Appendix B.1, and is therefore not detailed here.

Appendix C. Numerical bifurcation diagrams illustrating Figure 6 ($\varepsilon_1 = 0.01$). In this section, we present several bifurcation diagrams for fixed values of D, using S^0 as the bifurcation parameter. These diagrams illustrate the dynamical behaviours observed in the

various regions of the operating diagram shown in Figure 6 and summarized in Table 8, both obtained using the biological parameter values listed in Figure 2(d).

Table 14

Existence and stability of equilibria and limit cycles shown in Figures 15 to 17. The last column indicates the corresponding region in Figure 6 ($\varepsilon_1 = 0.01$) and describes the bifurcations occurring at the critical values σ_i, including the first Lyapunov coefficient l_1 at Hopf points.

Figure 15 ($D = 0.00902$)

S^0	E_0	E_1	C_1	C_2	C_3	Region & Bifurcation
$(0, \sigma_1)$	S					$\mathcal{R}_0$
$\sigma_1 \approx 16.527$						BP ($E_0 = E_1$)
(σ_1, σ_2)	U	S				$\mathcal{R}_1$
$\sigma_2 \approx 20.728$						Hopf ($l_1 \approx -1.204 \times 10^{-3}$)
(σ_2, σ_3)	U	U	S			$\mathcal{R}_2$
$\sigma_3 \approx 4997.917$						LPC ($C_2 = C_3$)
(σ_3, σ_4)	U	U	S	U	S	$\mathcal{R}_2^b$
$\sigma_4 \approx 4998.942$						LPC ($C_1 = C_2$)
(σ_4, σ_5)	U	U			S	$\mathcal{R}_2$
$\sigma_5 \approx 5002.427$						Hopf ($l_1 \approx -4.970 \times 10^{-8}$)
$(\sigma_5, +\infty)$	U	S				$\mathcal{R}_1$

Figure 16 ($D = 0.05$)

S^0	E_0	E_1	C_1	C_2	C_3	Region & Bifurcation
$(0, \sigma_1)$	S					$\mathcal{R}_0$
$\sigma_1 \approx 21.255$						BP ($E_0 = E_1$)
(σ_1, σ_2)	U	S				$\mathcal{R}_1$
$\sigma_2 \approx 42.975$						Hopf ($l_1 \approx -7.353 \times 10^{-6}$)
(σ_2, σ_3)	U	U	S			$\mathcal{R}_2$
$\sigma_3 \approx 1085.844$						LPC ($C_2 = C_3$)
(σ_3, σ_4)	U	U	S	U	S	$\mathcal{R}_2^b$
$\sigma_4 \approx 1414.44$						Hopf ($l_1 \approx -9.897 \times 10^{-8}$)
(σ_4, σ_5)	U	S	S	U		$\mathcal{R}_1^b$
$\sigma_5 \approx 2457.324$						LPC ($C_1 = C_2$)
$(\sigma_5, +\infty)$	U	S				$\mathcal{R}_1$

Figure 17 ($D = 0.06$)

S^0	E_0	E_1	C_1	C_2	C_3	Region & Bifurcation
$(0, \sigma_1)$	S					$\mathcal{R}_0$
$\sigma_1 \approx 22.635$						BP ($E_0 = E_1$)
(σ_1, σ_2)	U	S				$\mathcal{R}_1$
$\sigma_2 \approx 55.842$						Hopf ($l_1 \approx -2.151 \times 10^{-6}$)
(σ_2, σ_3)	U	U	S			$\mathcal{R}_2$
$\sigma_3 \approx 811.432$						LPC ($C_2 = C_3$)
(σ_3, σ_4)	U	U	S	U	S	$\mathcal{R}_2^b$
$\sigma_4 \approx 947.687$						LPC ($C_1 = C_2$)
(σ_4, σ_5)	U	U			S	$\mathcal{R}_2$
$\sigma_5 \approx 1224.732$						Hopf ($l_1 \approx -8.312 \times 10^{-8}$)
$(\sigma_5, +\infty)$	U	S				$\mathcal{R}_1$

C.1. Bifurcation diagram for $D = 0.00902$. The one-parameter bifurcation diagram with respect to S^0, for fixed $D = 0.00902$, corresponds to the horizontal line $D = 0.00902$ in the operating diagram shown in Figure 6. Figure 15 and Table 14 (for $D = 0.00902$) display five

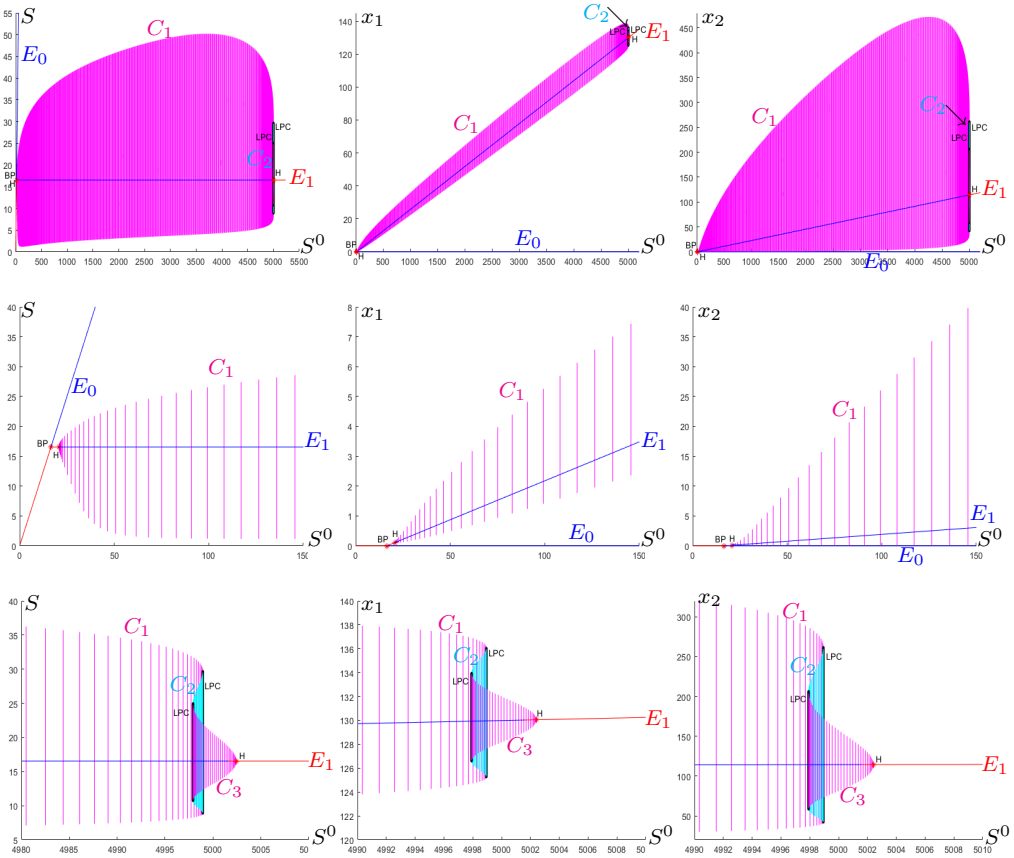

Figure 15. *Bifurcation diagram for the case $D = 0.00902$ (see Figure 6), showing equilibria and limit cycles as functions of S^0. The corresponding bifurcation values of S^0 are reported in Table 14.*

bifurcation values $\sigma_1 < \sigma_2 < \sigma_3 < \sigma_4 < \sigma_5$, corresponding to the intersections of the line $D = 0.00902$ with the BP, H, LPC, LPC, and H curves, respectively. The construction details of the bifurcation diagram in Figure 15 are similar to those described in Appendix B.1 and are therefore omitted.

For $S^0 \in (\sigma_3, \sigma_4)$, the system exhibits bistability between two stable limit cycles, C_1 and C_3, whose basins of attraction are separated by the two-dimensional stable manifold of the intermediate unstable limit cycle C_2. This dynamic corresponds to region $\mathcal{R}_2^b$ in Figure 6.

C.2. Bifurcation diagram for $D = 0.05$. The one-parameter bifurcation diagram with respect to S^0, for fixed $D = 0.05$, corresponds to the horizontal line $D = 0.05$ in the operating diagram shown in Figure 6. Figure 16 and Table 14 (for $D = 0.05$) display five bifurcation values $\sigma_1 < \sigma_2 < \sigma_3 < \sigma_4 < \sigma_5$, corresponding to the intersections of the line $D = 0.05$ with the BP, H, LPC, H, and LPC curves, respectively. The construction details of the bifurcation diagram in Figure 16 are similar to those provided in Appendix B.1 and are therefore omitted.

For $S^0 \in (\sigma_3, \sigma_4)$, the system exhibits bistability between two stable limit cycles, C_1 and C_3, whose basins of attraction are separated by the two-dimensional stable manifold of the unstable limit cycle C_2. This dynamic corresponds to region $\mathcal{R}_2^b$ in Figure 6. However, for

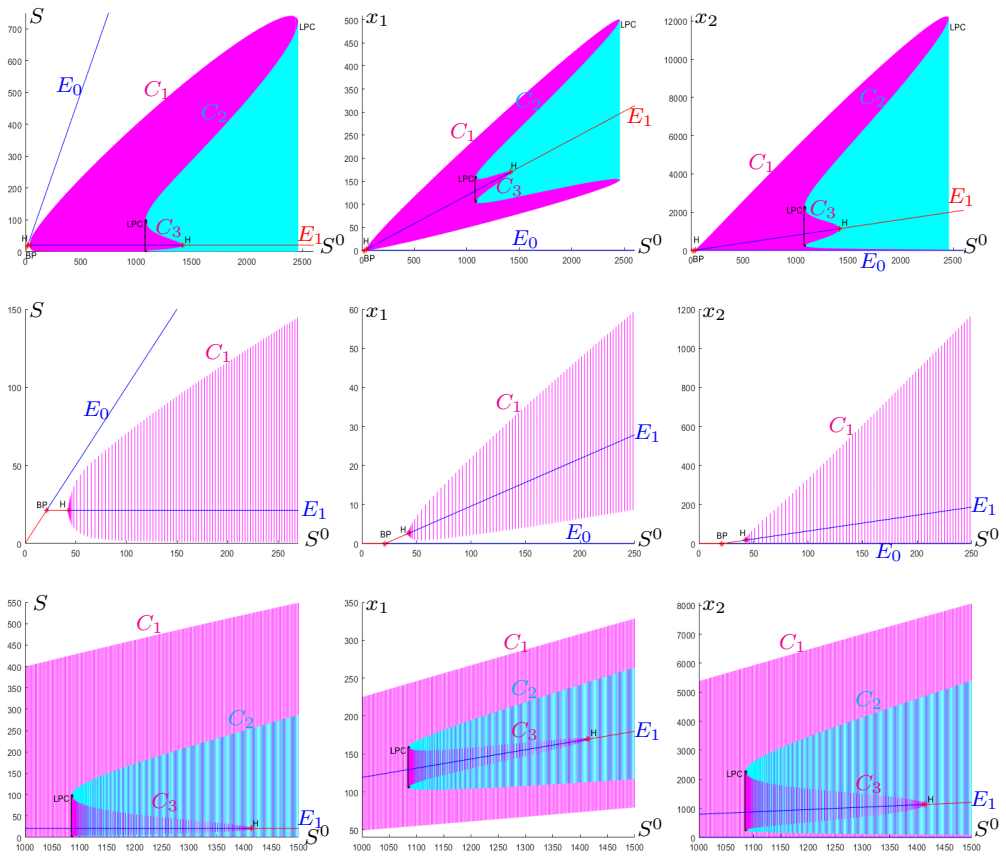

Figure 16. *Bifurcation diagram for the case $D = 0.05$ (see Figure 6), showing equilibria and limit cycles as functions of S^0. The corresponding bifurcation values of S^0 are reported in Table 14.*

$S^0 \in (\sigma_4, \sigma_5)$, the system displays bistability between the stable limit cycle C_1 and the positive equilibrium E_1. This behaviour corresponds to region $\mathcal{R}_1^b$ in Figure 6.

C.3. Bifurcation diagram for $D = 0.06$. The one-parameter bifurcation diagram with respect to S^0, for fixed $D = 0.06$, corresponds to the horizontal line $D = 0.06$ in the operating diagram shown in Figure 6. Figure 17 and Table 14 (for $D = 0.06$) display five bifurcation values $\sigma_1 < \sigma_2 < \sigma_3 < \sigma_4 < \sigma_5$, corresponding to the intersections of the line $D = 0.06$ with the BP, H, LPC, LPC, and H curves, respectively. The construction details of the bifurcation diagram shown in Figure 17 are similar to those described in Appendix B.1 and are omitted here.

For $S^0 \in (\sigma_3, \sigma_4)$, the system exhibits bistability between two stable limit cycles, C_1 and C_3, whose basins of attraction are separated by the two-dimensional stable manifold of the unstable limit cycle C_2. This dynamic corresponds to region $\mathcal{R}_2^b$ in Figure 6.

Appendix D. Bifurcation analysis for $\varepsilon_1 = 0.02$ (Figure 8). In this section, we present a series of bifurcation diagrams computed for fixed values of D, using S^0 as the bifurcation parameter. These diagrams illustrate the dynamical behaviours observed in the various regions

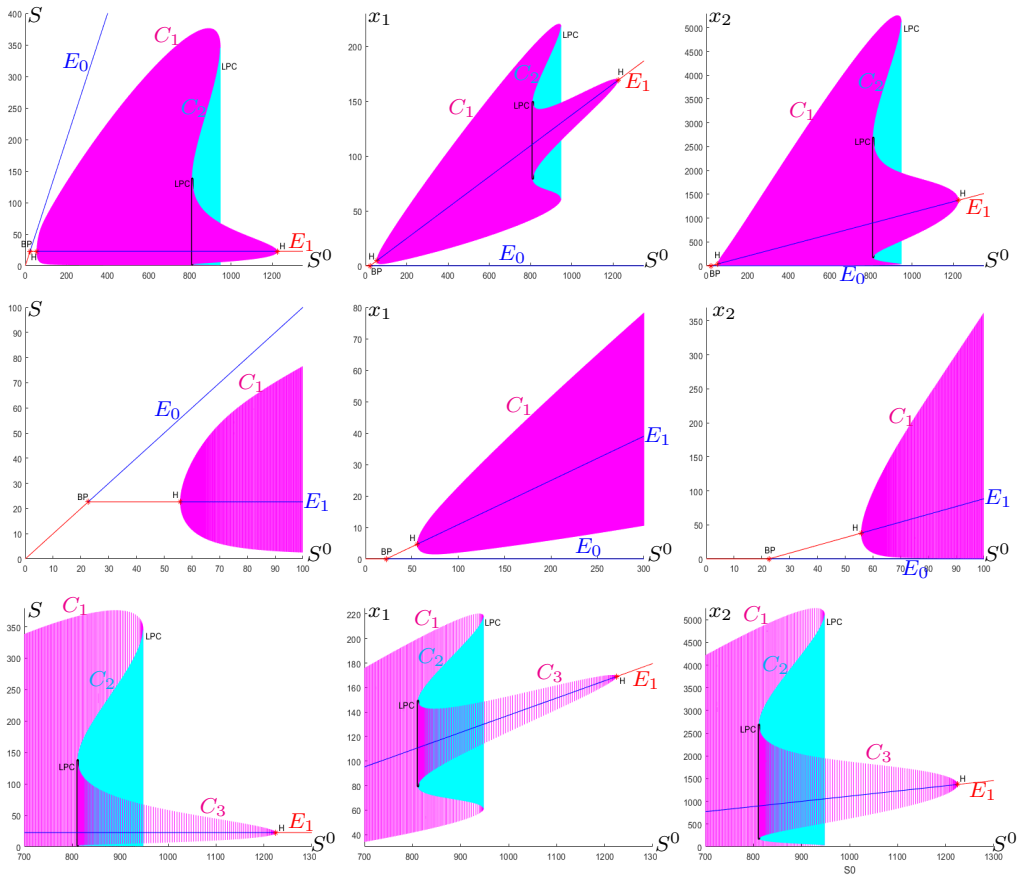

Figure 17. *Bifurcation diagram for the case $D = 0.06$ (see Figure 6), showing equilibria and limit cycles as functions of S^0. The corresponding bifurcation values of S^0 are reported in Table 14.*

of the operating diagram shown in Figure 8 and summarized in Table 8, which were obtained using the biological parameter values provided in Figure 2(e).

D.1. Bifurcation diagram for $D = 0.003$. The one-parameter bifurcation diagram with respect to S^0, for fixed $D = 0.003$, corresponds to the horizontal line $D = 0.003$ in the operating diagram shown in Figure 8. Figure 18 and Table 15 (for $D = 0.003$) display four bifurcation values $\sigma_1 < \sigma_2 < \sigma_3 < \sigma_4$, corresponding to the intersections of the line $D = 0.003$ with the BP, H, H, and LPC curves, respectively. The construction details of the bifurcation diagram in Figure 18 are similar to those described in Appendix B.1 and are omitted here.

For $S^0 \in (\sigma_3, \sigma_4)$, the system exhibits bistability between the stable limit cycle C_1 and the positive equilibrium E_1. This behaviour corresponds to region $\mathcal{R}_1^b$ in Figure 8. Note that the first Hopf bifurcation is supercritical, while the second is subcritical.

D.2. Bifurcation diagram for $D = 0.01$. The one-parameter bifurcation diagram with respect to S^0, for fixed $D = 0.01$, corresponds to the horizontal line $D = 0.01$ in the operating diagram shown in Figure 8. Figure 19 and Table 15 (for $D = 0.01$) display five bifurcation values $\sigma_1 < \sigma_2 < \sigma_3 < \sigma_4 < \sigma_5$, corresponding to the intersections of the line $D = 0.01$ with

Table 15

Existence and stability of equilibria and limit cycles shown in Figures 18 to 20. The last column indicates the corresponding region in Figure 8 ($\varepsilon_1 = 0.02$), along with the type of bifurcations occurring at the critical values σ_i, including the first Lyapunov coefficient l_1 at Hopf points.

Figure 18 ($D = 0.003$)

S^0	E_0	E_1	C_1	C_2	Region & Bifurcation
$(0, \sigma_1)$	S				$\mathcal{R}_0$
$\sigma_1 \approx 16.266$					BP ($E_0 = E_1$)
(σ_1, σ_2)	U	S			$\mathcal{R}_1$
$\sigma_2 \approx 18.318$					Hopf ($l_1 \approx -9.820 \times 10^{-4}$)
(σ_2, σ_3)	U	U	S		$\mathcal{R}_2$
$\sigma_3 \approx 16956.404$					Hopf ($l_1 \approx 3.874 \times 10^{-9}$)
(σ_3, σ_4)	U	S	S	U	$\mathcal{R}_1^b$
$\sigma_4 \approx 21412.460$					LPC ($C_1 = C_2$)
$(\sigma_4, +\infty)$	U	S			$\mathcal{R}_1$

Figure 19 ($D = 0.01$)

S^0	E_0	E_1	C_1	C_2	C_3	Region & Bifurcation
S^0	S					$\mathcal{R}_0$
$\sigma_1 \approx 16.962$						BP ($E_0 = E_1$)
(σ_1, σ_2)	U	S				$\mathcal{R}_1$
$\sigma_2 \approx 20.241$						Hopf ($l_1 \approx -5.026 \times 10^{-4}$)
(σ_2, σ_3)	U	U	S			$\mathcal{R}_2$
$\sigma_3 \approx 5571.279$						LPC ($C_2 = C_3$)
(σ_3, σ_4)	U	U	S	U	S	$\mathcal{R}_2^b$
$\sigma_4 \approx 5647$						Hopf ($l_1 \approx -1.110 \times 10^{-7}$)
(σ_4, σ_5)	U	S	S	U		$\mathcal{R}_1^b$
$\sigma_5 \approx 11627.456$						LPC ($C_1 = C_2$)
$(\sigma_5, +\infty)$	U	S				$\mathcal{R}_1$

Figure 20 ($D = 0.1$)

S^0	E_0	E_1	C_1	Region & Bifurcation
$(0, \sigma_1)$	S			$\mathcal{R}_0$
$\sigma_1 \approx 30.363$				BP ($E_0 = E_1$)
(σ_1, σ_2)	U	S		$\mathcal{R}_1$
$\sigma_2 \approx 285.777$				Hopf ($l_1 \approx -4.769 \times 10^{-8}$)
(σ_2, σ_3)	U	U	S	$\mathcal{R}_2$
$\sigma_3 \approx 631.178$				Hopf ($l_1 \approx -3.876 \times 10^{-8}$)
$(\sigma_3, +\infty)$	U	S		$\mathcal{R}_1$

the BP, H, LPC, H, and LPC curves, respectively. The construction details of the bifurcation diagram in Figure 19 are similar to those described in Appendix B.1 and are omitted here.

For $S^0 \in (\sigma_3, \sigma_4)$, the system exhibits bistability between two stable limit cycles, denoted C_1 and C_3, whose basins of attraction are separated by the two-dimensional stable manifold of the unstable limit cycle C_2. This behaviour corresponds to region $\mathcal{R}_2^b$ in Figure 8. In contrast, for $S^0 \in (\sigma_4, \sigma_5)$, the system exhibits bistability between the stable limit cycle C_1 and the positive equilibrium point E_1. This behaviour corresponds to region $\mathcal{R}_1^b$ in Figure 8.

D.3. Bifurcation diagram for $D = 0.1$. The one-parameter bifurcation diagram with respect to S^0, for fixed $D = 0.1$, corresponds to the horizontal line $D = 0.1$ in the operating diagram shown in Figure 8. Figure 20 and Table 15 (for $D = 0.1$) display three bifurcation

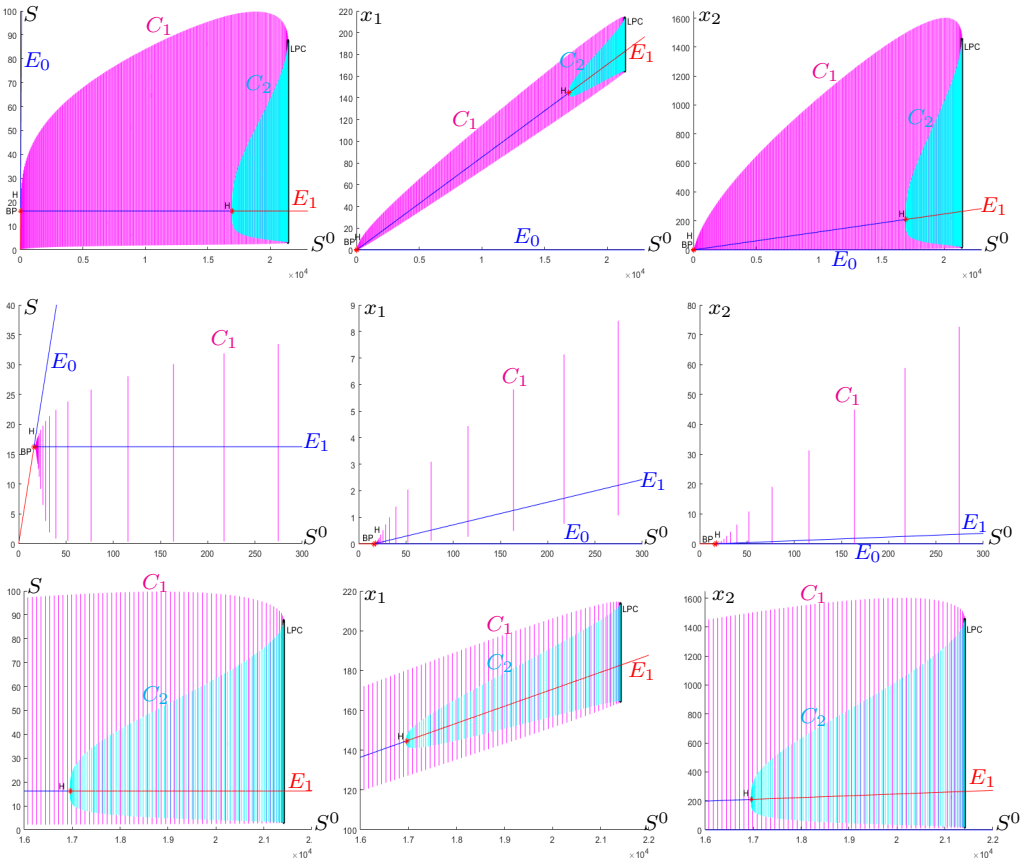

Figure 18. *Bifurcation diagram for the case $D = 0.003$ (see Figure 8), showing the equilibria and limit cycles as functions of S^0. The corresponding bifurcation values of S^0 are reported in Table 15.*

values $\sigma_1 < \sigma_2 < \sigma_3$, corresponding to the intersections of the line $D = 0.1$ with the BP curve and two Hopf bifurcation curves, respectively.

Acknowledgments. We warmly thank S.S. Pulyugin for his remarks and for the Lyapunov function used in the proof of Proposition 2.16. We thank the Euro-Mediterranean research network Treasure. A preliminary version of this work was prepared when TS was a member of the ITAP research unit (University of Montpellier, INRAE, Institut Agro, Montpellier, France). RFS thanks ITAP for hosting him with the financial support of CIMPA ("research in pairs"), and the Tunisian Ministry of Higher Education and Scientific Research (Young Researchers' Encouragement Program: 06P1D2024-PEJC).

REFERENCES

[1] M. Abell, J. Braselton and L. Braselton, A model of allelopathy in the context of bacteriocin production, Appl. Math. Comput., **183**, 916–931 (2006).

[2] R. Aris and A. E. Humphrey, Dynamics of a chemostat in which two organisms compete for a common substrate, Biotechnol. Bioeng., **19**, 1375–1386 (1977).

[3] B. C. Baltzis and A. G. Fredrickson, Competition of two microbial populations for a single resource in a

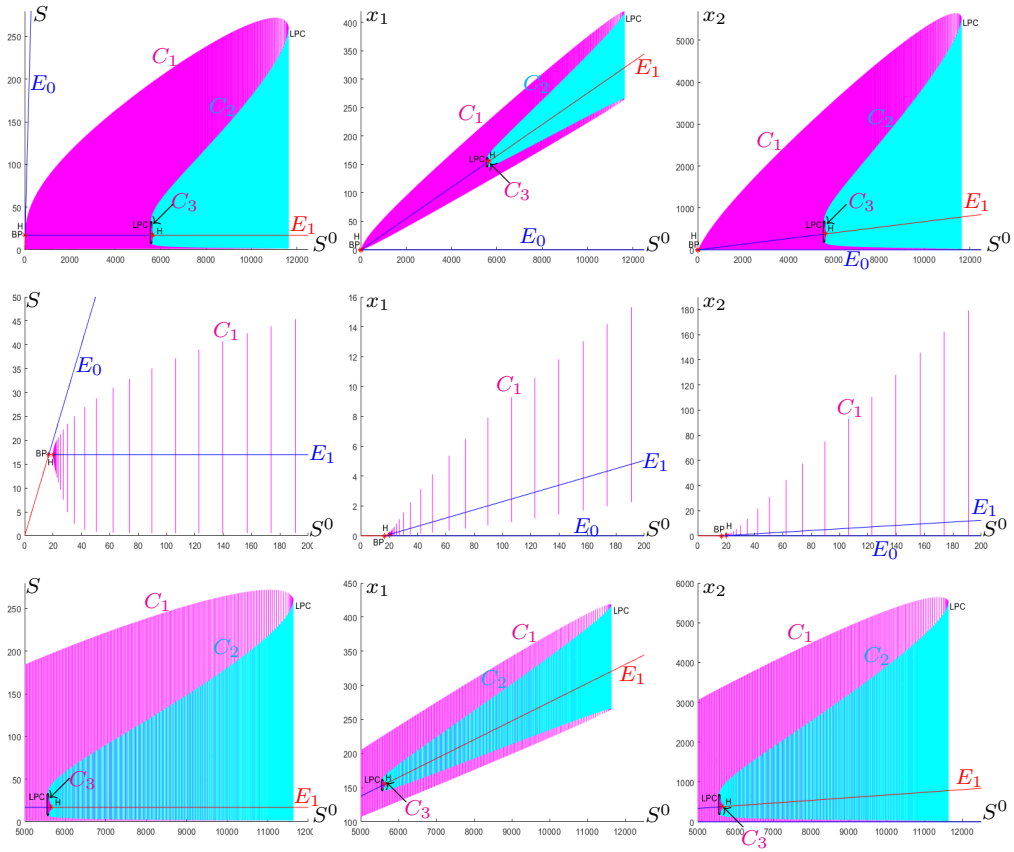

Figure 19. *Bifurcation diagram for the case $D = 0.01$ (see Figure 8), showing the equilibria and limit cycles as functions of S^0. The corresponding bifurcation values of S^0 are reported in Table 15.*

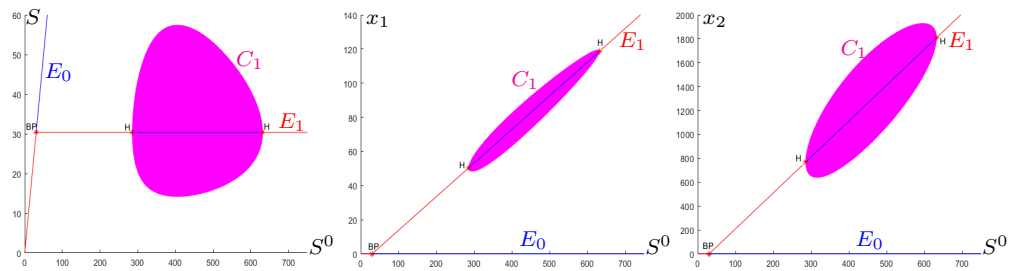

Figure 20. *Bifurcation diagram for the case $D = 0.1$ (see Figure 8), showing the equilibria and limit cycle as functions of S^0. The corresponding bifurcation values of S^0 are reported in Table 15.*

chemostat when one of them exhibits wall attachment, Biotechnol. Bioeng., **25**, 2419–2439 (1983).

[4] T. Bayen, H. Cazenave-Lacroutz and J. Coville, Stability of the chemostat system including a linear coupling between species, Discrete Contin. Dyn. Syst., Ser. B, **28**, 2014–2129 (2023).

[5] B. Benyahia, T. Sari and B. Cherki and J. Harmand, Bifurcation and stability analysis of a two step model for monitoring anaerobic digestion processes, J. Process Control, **22**, 1008–1019 (2012).

[6] A. Dhooge, W. Govaerts and Y. A. Kuznetsov, MATCONT: A Matlab package for numerical bifurcation

analysis of ODEs, ACM Trans. Math. Softw., **29**, 141–164 (2003).

[7] R. Fekih-Salem, Analysis of an intra- and interspecific interference model with allelopathic competition, J. Math. Anal. Appl., **542**, 128801 (2025).

[8] R. Fekih-Salem, Y. Daoud, N. Abdellatifi and T. Sari, A mathematical model of anaerobic digestion with syntrophic relationship, substrate inhibition and distinct removal rates, SIAM J. Appl. Dyn. Syst. (SIADS), **20**, 1621–1654 (2021).

[9] R. Fekih-Salem and T. Sari, Properties of the chemostat model with aggregated biomass and distinct removal rates, SIAM J. Appl. Dyn. Syst. (SIADS), **18**, 481–509 (2019).

[10] R. Fekih-Salem and T. Sari, A flocculation model in the chemostat with distinct removal rates and yields, J. Biol. Syst. (2025).

[11] A. G. Fredrickson and G. Stephanopoulos, Microbial competition, Science, **231**, 972–979 (1981).

[12] B. Haegeman and A. Rapaport, How flocculation can explain coexistence in the chemostat, J. Biol. Dyn., **2**, 1–13 (2008).

[13] J. Harmand, C. Lobry, A. Rapaport and T. Sari, The Chemostat: Mathematical Theory of Microorganism Cultures, Chemical Eng. Ser., ISTE-Wiley, New York (2017).

[14] P. A. Hoskisson and G. Hobbs, Continuous culture – making a comeback?, Microbiol., **151**, 3153–3159 (2005).

[15] S. B. Hsu, Limiting behavior for competing species, SIAM J. Appl. Math., **34**, 760–763 (1978).

[16] S. B. Hsu, S. Hubbell and P. Waltman, A mathematical theory for single-nutrient competition in continuous cultures of micro-organisms, SIAM J. Appl. Math., **32**, 366–383 (1977).

[17] P. De Leenheer, J. Dockery, T. Gedeon and S. S. Pilyugin, The chemostat with lateral gene transfer, J. Biol. Dynamics, **4**, 607–620 (2010).

[18] C. Lobry, La compétition dans le chemostat, in Des Nombres et des Mondes, Travaux En Cours 81, Éditions Herman, Paris, 119–187 (2012).

[19] J. Monod, La technique de culture continue, théorie et applications, Ann Inst Pasteur, **79**, 390–410 (1950).

[20] T. Mtar, R. Fekih-Salem and T. Sari, Mortality can produce limit cycles in density-dependent models with a predator-prey relationship, Discrete Contin. Dyn. Syst., Ser. B, **27**, 7445–7467 (2022).

[21] S. Nouaoura, R. Fekih-Salem, N. Abdellatif, T. Sari, Operating diagrams for a three-tiered microbial food web in the chemostat, J. Math. Biol., **85**, 7445–7467 (2022).

[22] A. Novick and L. Szilard, Description of the chemostat, Science, **112**, 715–716 (1950).

[23] S. S. Pilyugin and P. Waltman, The simple chemostat with wall growth, Siam J. Appl. Math. (SIAP), **59**, 1552–1572 (1999).

[24] A. Rapaport, Properties of the chemostat model with aggregated biomass, *Eur. J. Appl. Math.*, **29**, 972–990 (2018).

[25] T. Sari, Competitive Exclusion for Chemostat Equations with Variable Yields, Acta Appl Math, **123**, 201–219 (2013).

[26] T. Sari, Best Operating Conditions for Biogas Production in Some Simple Anaerobic Digestion Models, Processes, **2**, 258 (2022).

[27] T. Sari, Commensalism and syntrophy in the chemostat: a unifying graphical approach, AIMS Math., **9**, 18625–18669 (2024).

[28] T. Sari, The chemostat with lateral gene transfer and distinct removal rates, hal-05093107, Preprint (2025).

[29] H. L. Smith and P. Waltman, *The Theory of the Chemostat: Dynamics of Microbial Competition*, Cambridge University Press, Cambridge, UK (1995).

[30] L. Zou, X. Chen, S. Ruan and W. Zhang, Dynamics of a model of allelopathy and bacteriocin with a single mutation, Nonlinear Anal. Real World Appl., **12**, 658–670 (2011).